Impact of basement thrust fault on low-angle normal fault and rift basin evolution: a case study in the Enping sag, Pearl River Mouth Basin

Chao Deng[1], Rixiang Zhu[2, 1], Jianhui Han[3], Yu Shu[4], Yuxiang Wu[4], Kefeng Hou[5], Wei Long[3]

[1] State Key Laboratory of Continental Dynamics, Department of Geology, Northwest University, Xi'an 710069, China.
[2] Beitucheng West Road, Institute of Geology and Geophysics, Chinese Academy of Sciences, Chaoyang District, Beijing, 100029, China.
[3] College of Energy, Chengdu University of Technology, Chengdu, Sichuan 610059, China.
[4] Shenzhen Branch Company of CNOOC, Shenzhen, China.
[5] Changqing Oil Field, PetroChina Company Limited, CNPC, Xi'an, 710021, China.

Correspondence to: Chao Deng (dengchao@nwu.edu.cn), Rixiang Zhu (rxzhu@mail.igcas.ac.cn)

Abstract. Reactivation of pre-existing structures and their influence on subsequent rift evolution have been extensively analysed in previous researches on rifts that experienced multiple phases of rifting, where pre-existing structures were deemed to affect nucleation, density, strike direction and displacement of newly-formed normal faults during later rifting stage. However, previous studies paid less attention to the extensional structures superimposing on an earlier compressional background, leading to a lack of understanding, e.g., reactivation and growth pattern of pre-existing thrust fault as low-angle normal fault, and impact of pre-existing thrust fault on newly-formed high-angle faults and subsequent rift structure. This study investigating the spatial relationship between intrabasement thrust and rift-related faults in the Enping sag, northern South China Sea, indicates that the rift system is built on the previously deformed basement with pervasive thrusting structures, and that the low-angle major fault of the study area results from reactivation of intrabasement thrust fault. It also implies that reactivation mode of basement thrust faults is dependent on the overall strain distribution across rift, scale of basement thrust fault and strain shadow zone. In addition, reactivated basement thrust fault influences the nucleation, dip and displacement of nearby new faults, causing them to nucleate at or merge into it downwards, which are representative of the coupled and decoupled growth models of reactivated thrust fault and nearby new faults. This work not only provides insights into understanding the growth pattern of rift-related faults interacting with reactivated low-angle faults, but also has broader implications on how basement thrust faults influence rift structure, normal fault evolution and syn-rift stratigraphy.

1 Introduction

Reactivation of pre-existing basement faults or shear zones and their influence on the growth of newly-formed normal faults have been recognized in many multiphase rift basins, such as the NW Shelf of Australia (e.g., Frankowicz & Mcclay, 2010), Gulf of Thailand (e.g., Morley et al., 2004, 2007), Gulf of Aden (e.g., Lepvrier et al., 2002; Bellahsen et al., 2006), Northern

North Sea (e.g., Badley et al., 1988; Færseth, 1996; Færseth et al., 1997; Odinsen et al., 2000; Whipp et al., 2014; Duffy et al., 2015; Deng et al., 2017a; Fazlikhani et al., 2017), and East African Rift (Le Turdu et al., 1999; Lezzar et al., 2002; Corti, 2009; Muirhead & Kattenhorn, 2017). Previous researches suggested that pre-existing basement faults or shear zones originated from an earlier tectonic event were prone to reactivate, interact and link with newly-formed normal faults during a later rifting stage, and finally resulted in some special structural styles, e.g., non-collinear fault arrays, various styles of fault interactions, and gradual change in fault geometries with increased depth (e.g., Morley et al., 2004, 2007; Duffy et al., 2015; Phillips et al., 2016). In addition, our understanding of three-dimensional fault geometry and evolution affected by pre-existing basement weaknesses or faults has been greatly improved by a number of studies using physical analogue and numerical models (e.g., McClay and White, 1995; Keep and McClay, 1997; Bellahsen and Daniel, 2005; Henza et al., 2010, 2011; Chattopadhyay and Chakra, 2013; Henstra et al., 2015; Deng et al., 2017b, 2018; Zwaan and Schreurs, 2017; Molnar et al., 2019; Maestrelli et al., 2020; Gouiza et al., 2021; Samsu et al., 2021; Wang et al., 2021; Zwaan et al., 2021). Based on those researches, people notice that a pre-existing basement fault can reactivate in variable modes as a response of a changing strain magnitude and/or extension direction, and play an important role on the geometry of neighbouring new faults, such as fault density, orientation and displacement (e.g., Morley et al., 2004, 2007; Henza et al., 2010, 2011; Deng et al., 2017b, 2018). However, previous studies stressed more attention to the rift basins that evolved through multiple phases of rifting, yet the characteristics of extensional structures developing after a period of compressional event, such as reactivation mode of pre-existing thrust faults, growth pattern of low-angle normal faults and their interactions with high-angle normal faults, still remain short of investigation. Many rifts are found to be underlain and affected by basement thrusting structures (Bonini et al., 2015, 2019; Del Ventisette et al., 2021); thus, analysing their evolution during later rifting will deepen our understanding of inherited structures.

The South China Sea, located at the junction area of the South China Block, Indo-China Block and Pacific Plate (Fig. 1), is known as a Late Cretaceous to Early Cenozoic rift system that was built on a previously deformed basement containing pre-existing thrust and strike-slip faults, due to negative inversion from compressional to extensional tectonic setting during the Late Mesozoic (e.g., Holloway, 1982; Taylor and Hayes, 1983; Li and Li, 2007; Li et al., 2012; Shi and Li, 2012). The influence of pre-existing basement structures on the rift basin evolution of the northern South China Sea has already been reported by previous researchers. For example, Hu et al. (2013) argued that the tectonic evolution of the Qiongdongnan Basin was controlled by faults reactivated from NE-SW- and E-W-trending pre-existing fabrics. Also, Ye et al. (2020) suggested that the overall rift architecture in the proximal domain of the northern South China Sea margin is mainly controlled by reactivation of two pre-existing fault systems within the basement, such as the WNW- to EW- and the ENE-striking pre-existing faults. However, there are still some key issues concerning about the evolution of the fault network and rift basins. For instance, how does pre-existing thrust fault reactivate and grow as a low-angle normal fault during the subsequent rifting? How does pre-existing thrust fault control the development of newly-formed normal faults and rift basins? Answering those questions will help to improve our understanding of the structural style and rift development over pre-existing basement thrusting structures in general.

In this contribution, the Enping sag in the Pearl River Mouth Basin is selected as the starting point for elucidating the influence of pre-existing basement thrusting structures on normal fault and rift basin development (Fig. 1c). Firstly, we integrate the 3D seismic reflection and borehole data in the study area to interpret the geometry of basement thrust faults and their spatial relationship with rift-related normal faults. On this foundation, the kinematics of pre-existing basement structures and newly-formed normal faults, as well as their interactions are analysed according to throw variation information. The objective of this step is to figure out the growth and interaction styles between pre-existing basement thrust faults and newly-formed normal faults, along with fault evolution of the study area. At the second step, we try to explore the reactivation mode of basement thrust faults and the factors controlling their reactivation and rift development in the northern South China Sea. Finally, we discuss about the impacts of basement thrust faults on the newly-formed fault growth and rift development during a subsequent rifting stage in general. Through detailed study of the basement and rift-related structures, this work will not only provide insights into understanding the fault growth pattern with interactions between high-angle rift-related faults and low-angle basement thrust faults, but also have broader implications on how basement thrust faults influence rift basin development.

2 Geological setting

The South China Sea is a tectonically complex area that has been affected by both collision of the Indo-China Block and subduction of the paleo-Pacific Plate toward the SW and SE boundaries of the South China Block, respectively (e.g., Charvet et al., 1994; Li, 2000; Zhou et al., 2006; J. Li et al., 2014; Z. Li et al., 2014). The pre-Cenozoic evolution of the South China Sea area was mainly controlled by two periods of regional tectonic movement: the Indosinian movement (251–205 Ma) and the Yanshanian movement (180–67 Ma) (Zhou et al., 2006). The Indosinian movement was dominated by the orogeny and suture between the South China Block and the Indochina Block, causing the formation of NW-SE-trending thrust and strike-slip faults at the western margin of the South China Block (Metcalfe, 2006). The Yanshanian movement was driven by NW subduction of the paleo-Pacific Plate beneath the South China Block, and was structurally characterized by E-W- to NE-SW-trending thrust and strike-slip faults (Faure et al., 1996; Shu et al., 2006; Zhou et al., 2006). At the end of the Yanshanian movement, the South China Block underwent a tectonic transition from compressional to extensional setting, which is supposed to result in the onset of continental rifting from c. 60Ma or even earlier (Holloway, 1982; Taylor and Hayes, 1983; Li and Li, 2007; Li et al., 2012; Shi and Li, 2012). During the Cenozoic, the South China Sea area experienced a long episode of intense continental rifting, breakup and seafloor spreading, producing numerous extensional basins that were infilled with a large volume of red fluvial and lacustrine sediments known as Red Beds (e.g., Li, 1999; Shu et al., 2009; J. Li et al., 2014). Previous studies indicated that the Cenozoic rift evolution of the South China Sea was featured by episodic rifting, with a clockwise rotation of the extension direction (e.g., Ru and Pigott, 1986; Pigott & Ru, 1994; Zhou et al., 1995). Two main rifting episodes have been identified in the Enping sag with confidence: i) the Early Eocene rifting (49-39 Ma, Episode 1, Fig. 2), and ii) the Late Eocene to Early Oligocene rifting (39-32 Ma, Episode 2, Fig. 2). During the Early Eocene rifting episode, the extension direction was assumed to be NNW-SSE, leading to the development of NE(E)-SW(W) -trending normal faults

and the deposition of the Wenchang Formation. During the Late Eocene to Early Oligocene rifting episode, there had a clockwise rotation of the extension direction to nearly N-S, which caused the development of NEE- or E-W-trending normal faults and the deposition of the Enping Formation. Rift activity ceased when continental breakup occurred and seafloor spreading began at ca. 32 Ma, and thereafter, the South China Sea entered the post-rift stage that was dominated by regional thermal subsidence (e.g., Li, 1993; Sun et al., 2014; Wu et al., 2014).

The Enping Sag is an overall NE-SW-trending negative zone in the Pearl River Mouth Basin at the northern margin of the South China Sea (Fig. 1). The NW and SE boundaries of the Enping Sag are defined by the Northern Uplift Zone and Panyu Lower Uplift, respectively; and in the NE and SW, it gradually transfers to the neighbouring sags through NW-trending structures. In a smaller scale, the Enping sag is further divided into three sub-sags: Ep12, Ep17, and Ep18 sub-sags (Fig. 1c, Ye et al., 2018). The Ep12 and Ep17 sub-sags are bounded in the northwest by the NE-SW-striking major fault F1, whereas the Ep18 sub-sag is bounded in the north by the E-W-striking major fault F2 (e.g., Xu et al., 2014; Shi et al., 2015). The syn-rift stratigraphic units include the Wenchang and Enping Formations (Fig. 2). The Wenchang Formation that directly overlies the top basement mainly consists of grey to black organic-rich shale interbedded with sandstone being deposited in middle to deep lacustrine, corresponding to the Early Eocene rifting episode (Fig. 2). The overlying Enping Formation is composed of shale, sandstone, and thin coal beds from fluvial to shallow and middle lacustrine, representing the deposition of the Late Eocene to Early Oligocene rifting episode (Fig. 2; Liu et al., 2016). Post-rifting strata start from the Zhuhai Formation, which gradually transforms to marine facies as a result of continental breakup (e.g., Li, 1993; Sun et al., 2014; Wu et al., 2014).

3 Data and methods

Structural interpretation and mapping are performed using the 3D seismic cube and wellbore data covering the study area, which are provided by the Shenzhen Branch of CNOOC of China (Fig. 1). The 3D seismic cube has an area of ~2300 km^2 with a line spacing of 12.5 m, and images down to ca. 6 s TWT in depth. The seismic reflection is displayed in normal polarity (SEG Convention), whereby a downward increase in acoustic impedance is indicated by a peak (brown reflection) and a decrease in acoustic impedance is represented by a trough (black reflection) (Figs. 2 and 3). In addition, two of the drilled wells are tied to the seismic section by means of synthetic seismograms, which is sufficient for tracing and mapping the horizons in the study area (Fig. 3). Well-18 drills through the syn-rift strata and penetrates into the basement, while the other wells stop within the syn-rift strata.

Three key seismic horizons, i.e., T_g, T_{80} and T_{70} from bottom to top, are mapped for establishing the overall structural framework (Fig. 2). Among them, T_g horizon is a very strong and continuous reflector that separates the overlying layered reflections from the underlying chaotic reflections, indicating that it is a regional angular unconformity representing the rift onset; thus, we define it as the top of the crystalline basement (Fig. 2; Ru and Pigott, 1986; Li et al., 1999; Yan et al., 2014). T_{70} horizon is a strong reflector that is located close to the ceiling of the wedge-shaped growth stratigraphy, i.e., the T_g to T_{70} interval, representing the breakup unconformity formed in response to the continental breakup and incipient seafloor spreading

of the South China Sea; thus, we define it as the top of the syn-rift stratigraphic units (Fig. 2). T_{80} horizon is located at the interface between the Wenchang and Enping Formations according to the seismic-well tie, so is defined as a local angular unconformity within the syn-rift stratigraphy that separates the Wenchang from the Enping Formations (Figs. 2 and 3).

The key structures developing in the study area are classified into two groups: the intrabasement structure and the rift-related cover structure that are separated from each other by the top basement or T_g horizon (Fig. 4). The intrabasement structure is identified according to the strong seismic reflection packets that are constrained within the crystalline basement (Fig. 4b). Because of limited lateral continuity of seismic reflectors within the basement, the intrabasement structure is mainly portrayed in cross-sectional view, with the goal of displaying their geometric style and spatial relationship with the cover structures. The rift-related cover structure, however, is primarily interpreted according to the offset of the continuous reflectors in the stratigraphic package, and is described in regard to fault length, strike, dip and throw (Fig. 4c). The relative dip angle of the faults is estimated from the cross-sections in TWT that are stretched to a suitable scale for the cover faults in the post-rift strata dipping at c. 60º, as seen in depth-migrated ones.

On the basis of the structural interpretation and mapping, we employ two commonly-used methods to analyse the fault kinematics: i) throw-length (T-x) plots that show fault throw (T) against the distance (x) along fault strike are used to study the propagation and linkage history of fault segments (e.g., Peacock and Sanderson, 1991; Cartwright et al.,1995; Dawers and Anders,1995; Gupta and Scholz, 2000; Baudon and Cartwright, 2008); ii) throw-depth (T-z) profiles that display fault throw (T) against depth (z) can be employed to interpret fault propagation history in vertical (e.g., Cartwright et al., 1998; Baudon and Cartwright, 2008).

4 Structural style and fault geometry

4.1 Intrabasement structure

We discover two types of strong seismic reflections within the crystalline basement. The first type of intrabasement reflections (Type I) is a relatively linear, thin (c. 10-100 ms TWT), high-amplitude reflection packet that is composed of a trough-peak-trough wave assemblage in cross-section (Figs. 4 and 5). The second type of intrabasement reflections (Type II) is characterized by a package of relatively winding, thick (c. 500-1000 ms TWT), medium- to high-amplitude reflections (Fig. 5c).

Type I intrabasement reflections, e.g., BF1 in the hanging wall of the rift-related fault F1, BF2 and BF3 in the footwall of fault F3, BF4 and BF5 in the footwall of fault F4, and BF6 in the footwall of fault F6 at the eastern border of the study area, etc., are dominantly dipping at <30º toward SE, with a lateral spacing of c. 500 m between each other (Figs. 5 and 6d). Also, most of Type I intrabasement reflections tip-out at or below the top basement, except that the upper tip of intrabasement reflection BF2 exactly extends above T_g horizon and offsets a few reflection waves in the stratigraphic cover (Fig. 5b). It is uncertain about where the lower tip of Type I intrabasement reflections terminates due to poor seismic imaging at the depth larger than 4 s TWT, but some of them may extend downward and connect with shear zones in the lower crust. In addition, we observe that intrabasement reflection BF3 merges into the plane of fault F3 with increased depth, and has approximately the same dip

angle and seismic reflection characteristic with the lower part of fault F3 in the basement rock (Fig. 5b). These observations confirm that Type I reflections represent real geological boundaries rather than acquisition- or processing-related geophysical artefacts.

In comparison, a set of high-amplitude, folded or winded, Type II intrabasment reflections develop to the SE of Type I reflection BF4 at the depth of c. 3-4 s TWT, resembling a fault propagation folding related to thrust faulting structure (Fig. 5c). In addition, we observe that the bottom of Type II reflections is displaced by some Type I intrabasement reflections, having an up-dip offset of c. 50 ms TWT (Fig. 5c). Similar characteristics are also observed in the footwall of fault F6, where a group of Type II intrabasement reflections are folded and displaced by Type I intrabasement reflections (Fig. 6d). Although the top and bottom of Type II reflections can be sketched in cross-section, it is too challenging to trace them across the study area because they have bad lateral continuity.

Based on the observations described above, we interpret Type I intrabasement reflections to be pre-existing basement faults, i.e., basement faults BF1-BF6. According to the deformation manner of Type II intrabasement reflections, they are suggested to be pre-existing basement thrust faults originated from the compressional tectonics prior to the Late Cretaceous to Early Cenozoic extensional event. There are three evidences supporting our interpretation: i) termination of the upper tip of Type I intrabasement reflections against or beneath the top basement, such as BF1 and BF3, indicating that they are pre-existing faults forming before the initiation of the Late Cretaceous to Early Cenozoic rifting stage; ii) fault propagation folding structure that occurs close to the basement faults BF4 and BF6, implying that folding structure is the immediate result of reverse fault movement; and iii) reverse offset of Type II intrabasement reflections across Type I intrabasment reflections, which is a good representative of up-dip slip of reverse fault (Figs. 5 and 6). For other basement faults, it is difficult to measure their displacement owing to the lack of traceable strong reflections across them; thus, it is less possible to determine their sense of shear. Based on the aforementioned evidences, we suggest that there exist a number of NE-SW- or E-W-striking thrust faults in the basement of the Enping sag, which are supposed to be associated with the compressional event prior to the Late Cretaceous to Early Cenozoic rifting. This suggestion is consistent with previous studies in relation to the development of basement thrust faults (e.g., Nanni et al., 2017; Ye et al., 2020).

4.2 Rift-related cover structures

The Late Cretaceous to Early Cenozoic rift structure is dominated by two major faults that are >15 km in length and >200 ms TWT of maximum throw, namely the NE-SW-striking major fault F1 and the approximately E-W-striking fault F2 lying in the hanging wall of fault F1 (Fig. 7). The western end of the major fault F2 terminates against the middle part of major fault F1, exhibiting a connected fault array at the top basement. The major faults bound three separated syn-rift half-grabens, i.e., the Ep12, Ep17 and Ep18 sub-sags, in the hanging wall of the eastern and western parts of fault F1, and fault F2, respectively. Apart from the major faults, there also develop a few numbers of minor faults that are <15 km in length or <200 ms TWT of maximum throw in the hanging wall of the major faults (Figs. 6 and 7). Following sections are detailed description of the geometry and structural relationship between the major and minor faults.

4.2.1 Major faults

The major fault F1 has a length of c. 60 km and a dominant NE-SW strike, but makes a bend as it turns to nearly N-S at its westernmost end (Fig. 7). In addition, the cross-sectional geometry of the major fault F1 and the corresponding hanging-wall stratigraphy significantly changes along strike. In the southwest, for example, fault F1 is at ~10º dips toward SE and shows a 'ramp-flat' shape in cross-section view (Fig. 6a). The upper tip of fault F1 terminates close at T_{70} horizon, while the lower tip penetrates into the basement and extends southward beyond the study area, making a vertical offset of c. 1500 ms TWT at T_g horizon (Fig. 7). In the hanging wall of fault F1, i.e., the Ep17 sub-sag, the NW-expanding stratigraphic wedge between T_g and T_{70} horizons is c. 1700 ms TWT thick and c. 35 km wide in maximum. In the central part, however, the shape of fault F1 is approximately listric from top to bottom, with a gentle dip at c. 10º (Fig. 6b). In addition, the upper tip of fault F1 reaches above T_{70} horizon, and its lower tip extends into the basement, creating a vertical offset of c. 1000 ms TWT at T_g horizon (Fig. 7). The stratigraphic interval between T_g and T_{70} horizons, c. 1200 ms TWT of thickness in maximum, is featured by a package of sub-tabular stratigraphy that gradually overlaps the slipping plane of fault F1. In the northeast part of fault F1 where the Ep12 sub-sag is located, the geometries of the fault plane and hanging-wall stratigraphy are in sharp contrast with the previous parts. Firstly, fault F1 shows a 'dogleg' shape in cross-section, with its upper portion at c. 15º dips and the lower portion at c. 10º dips (Fig. 6c). Secondly, the upper tip of fault F1 terminates at T_{80} horizon, and its lower tip extends downward into the basement, making a vertical offset of c. 800 ms TWT at Tg horizon (Fig. 7). Thirdly, the T_g to T_{80} stratigraphic interval in the hanging wall of fault F1 is also characterized by a wedge-shaped growth package, but it is only c. 800 ms TWT thick and c. 8 km wide in maximum. Fourthly, significant rollover or rotation of stratigraphic beds occurs in the hanging-wall block, accompanied by erosion of the T_g to T_{80} stratigraphy at the crest of the fault block. Finally, the overlying T_{80} to T_{70} stratigraphic package, only c. 300 ms TWT of thickness, is approximately tabular and unaffected by fault F1 (Fig. 6c). Going further east, there develops an intrabasement fault BF6 of which the position coincides with the northeast extension line of the major fault F1. However, the top basement and the stratigraphic beds above intrabasement fault BF6 have no offset, suggesting that the major fault F1 does not propagate into this section (Fig. 6d). In the footwall of fault F1, there is no much difference in the stratigraphic pattern along strike, because the top basement is almost horizontal and overlain by a tabular stratigraphic package. As a whole, we observe a NE-trending decrease in the final offset of the major fault F1 (Fig. 7). Also, the thickness and width of the overlying syn-rift stratigraphy also decrease from SW to NE. Such a smaller volume of the syn-rift stratigraphy in the Ep12 sub-sag compared to the Ep17 sub-sag is possibly related to the synchronous growth of fault F2 with fault F1 in the eastern part of the Enping sag.

The major fault F2 is c. 20 km long, nearly E-W-striking and S-dipping in map view (Fig. 7). Fault F2 is situated in the hanging wall of major fault F1, with its western tip terminating against the major fault F1 and its eastern tip extending away from the major fault F1. In cross-section, fault F2 has a steeper dip than fault F1, with a listric shape from top to bottom (Fig. 6c). In details, the upper part of fault F2 is at c. 45º dips and extends upward to the surface of the stratigraphic beds, whereas its lower part gradually becomes gentler and ends up joining into the more shallowly-dipping major fault F1 at depth. In addition, the

T_g to T_{70} stratigraphic interval in the hanging wall of fault F2 is characterized by a thick wedge-shaped growth package that has a maximum thickness of c. 1600 ms TWT. In contrast, the stratigraphic package above T_{70} horizon has an approximately tabular shape (Fig. 6c). Similar to the northeast part of fault F1, prominent rollover and/or rotation of the stratigraphic package is also observed in the hanging wall of fault F2.

4.2.2 Minor faults

Minor faults, c. 5 km long, E-W-striking and at ~60º dips in general, are mostly distributing in the hanging wall of the major faults F1 and F2 (Fig. 6). Different from the major faults, minor faults mainly occur in the stratigraphic cover. For instance, the upper tip of the majority of the minor faults extends above T_{70} horizon, and the lower tip of them terminates above the top basement, i.e., fault F5 (Fig. 6b). Also, there are some minor faults that penetrate deep into the basement, i.e., faults F4 and F7 (Fig. 6a). In addition, the stratigraphic package across the minor faults is roughly tabular. In specific, abrupt changes in the thickness of the stratigraphic package below T_{70} horizon are observed across some minor faults, i.e., faults F4 and F7 (Fig. 6a). In contrast, there are few distinct thickness variations for the stratigraphic package above T_{70} horizon.

In cross-section, minor faults display different assembling styles on the two oppositely-dipping slopes of the Enping sag. On the northern slope that is controlled by the major fault F1, we observe that minor faults arrange at a regular spacing of c. 2000 m and preferentially dip toward the downdip direction of the major fault F1 (Fig. 8a). This characteristic assemblage style generates a set of domino faults standing on top of the major fault F1. In comparison, on the southern slope that is much gentler, minor faults are either northward or southward dipping, leading to a random distribution of several couples of conjugate faults in the stratigraphic cover (Fig. 8b). Such variation in the assemblage style of minor faults is closely related to the downdip slip of the gently-dipping major fault F1, which is favourable for newly-formed minor faults to dip toward the slip direction of the underlying major fault.

5 Relationship between the low-angle and high-angle normal faults

Based on the fault geometry described above, we note that the rift-related faults can be divided into low-angle (<30º dip) and high-angle (>30º dip) normal faults. Low-angle normal fault is represented by the major fault F1, whereas most of the other faults are high-angle normal faults, e.g., fault F2. In addition, the high-angle normal faults interact with the low-angle normal fault in various styles, including: i) 'isolated fault' that forms independently from and are unaffected by the low-angle fault, ii) 'merging faults' that join together at the lower tips, iii) 'abutting fault' that initiates at the low-angle fault, and iv) 'cross-cutting fault' that offsets the low-angle fault. Each of the fault interaction styles is described below in details, focusing on the cross-sectional geometry and interaction manner.

5.1 Isolated fault

The first style of fault interaction, i.e., isolated fault, is represented by the relationship between the high-angle fault F7 and the low-angle major fault F1, and is the standard for comparison with other interaction styles. It is observed that the high-angle fault F7 is located far away from and has no interaction with the low-angle major fault F1 (Figs. 6a and 7), suggesting that the major fault F1 plays little effect on the growth of fault F7. Similarly, this style of fault interaction and the evolution have been described in numerous studies about the interactions between pre-existing and newly-formed faults (cf. Duffy et al., 2015; Phillips et al., 2016; Deng et al., 2017b; Fazlikhani et al., 2017).

5.2 Merging faults at the lower tips

Merging faults are represented by the relationship between faults F1 and F2, with the high-angle fault F2 occurring in the hanging wall of the low-angle fault F1 (Fig. 9a). The lower part of fault F2 becomes shallower at dip and merges into the plane of fault F1 at the depth of c. 4 s TWT, from where fault F2 shares one common slipping plane with fault F1 toward the southeast. The upper tip of fault F1 terminates at T_{80} horizon and bounds a wedge-shaped growth package between T_g and T_{80} horizons, which is overlain by a tabular stratigraphic package between T_{80} and T_{70} horizons. In contrast, fault F2 bounds a thicker wedge-shaped growth package comprising the stratigraphy from T_g to T_{70} horizon. This observation indicates that faults F1 and F2 initiated during the early stage of the rifting, but fault F2 had a longer active history than fault F1, possibly because of their downward linkage during the late stage of rifting. Accordingly, the evolution of 'merging faults' is composed of three stages: i) high-angle fault initiates within the hanging wall of active low-angle major fault; ii) high-angle fault becomes gentler as it propagates downwards owing to interaction with low-angle major fault; and iii) high-angle fault merges into the low-angle fault and continues slipping toward the downdip direction, resulting in abandonment of the upper part of low-angle fault. Such growing history of merging faults resembles the 'merging fault interaction' described in previous studies about the relationship between intrabasement shear zone and rift fault (e.g., Phillips et al., 2016; Fazlikhani et al., 2017). They indicated that intrabasement shear zone acted to perturb the regional stress field and localize strain, causing fault nucleation within its hanging wall, and physically link with the underlying structure.

5.3 Abutting fault initiating at the low-angle normal fault

Abutting fault is represented by the relationship between faults F4 and F1. At T_g horizon, fault F4 is situated in the footwall of fault F1, with its eastern tip terminating right at the plane of fault F1 (Fig. 7), which is very similar to the abutting interaction observed in previous studies (e.g., Duffy et al., 2015; Deng et al., 2017). In the cross-section traversing the intersection point of faults F1 and F4, the low-angle fault F1 tips out at the intersection point, from where fault F4 is divided into two segments (Fig. 9b). The upper segment is roughly linear at ~60° dips, and bounds a sub-tabular stratigraphic package above T_{70} horizon in the hanging wall, whereas the lower segment displays a listric shape in the basement. T-z profile shows that the maximum throw of fault F4, c. 350 ms TWT, is located at the point intersecting with fault F1, from where fault throw decreases upwards

(Fig. 10a), excluding the lower segment because of no discernible reflectors within the basement. Those observations suggest that fault F4 initiated at the upper tip of the low-angle fault F1 and then propagated outwards at a larger dip. Similar characteristics are also observed for the relationship between the domino faults and the major fault F1. For instance, fault F5 gradually follows the slipping plane of the major fault F1 with increased depth and has the maximum throw of c. 150 ms TWT at the intersection point with fault F1 on T-z profile (Fig. 10b). Such characteristics indicate that the domino faults and fault F4 initiate at and then propagate outwards from the plane of fault F1, and that the underlying fault F1 acts as a basal decollement for the domino faults and fault blocks to slip on top of it.

5.4 Fault cross-cutting the low-angle fault

There have a few cases that high-angle and low-angle faults are originally unrelated, with the former cross-cutting the latter afterwards. For instance, the roughly linear fault F8 is situated on the gentle slope of the half-graben, with its upper tip extending above T_{70} horizon and its lower tip penetrating into the basement (Fig. 9c). Especially, fault F8 cross-cuts and displaces the trace of the low-angle major fault F1 at the depth of c. 4 s TWT, generating a vertical offset of c. 200 ms TWT. T-z profile shows that the maximum throw of fault F8, i.e., c. 300 ms TWT, occurs at T_g horizon, from where throw value has a decreasing trend upwards (Figs. 9c and 10c). In addition, the stratigraphy in the hanging wall of fault F8 is composed of a wedge-shaped growth package between T_g and T_{80} horizons and a tabular package above it. The observations suggest that the high-angle fault F8 started to be active during the early stage of the rifting, and experienced a three-step growth history: i) nucleation of high-angle fault above low-angle fault, ii) fault propagation upward and downward, and iii) ultimate cross-cutting of the underlying low-angle fault. This case illustrates that high-angle fault initiated above and eventually offset the underlying low-angle fault, which is typical for cross-cutting interaction.

6 Discussion

This study uses seismic reflection data to interpret the geometric relationship and evolution of intrabasement and rift-related structures in the Enping sag, the northern South China Sea. The fault network is characterized by a double-layer structure: the intrabasement thrusting faults at the bottom layer and the rift-related extensional faults in the upper stratigraphic layer. After examining the geometric style and spatial distribution of intrabasement and rift-related cover structures, we find that the intrabasement thrust faults have different kinematics from the rift-related cover structures, indicating that the former are pre-existing structures formed before the rifting. In addition, we observe that the rift-related structures are dominated by a low-angle major fault, which interacts with high-angle normal faults in various styles and affects the geometry of neighbouring new faults. Following discussion will reveal how basement thrust fault evolves and influences the rift-related fault growth and rift system development during the subsequent rifting.

6.1 Mechanism of the low-angle normal fault development in the northern South China Sea

Normal fault initiated in the brittle upper crust is generally at ~60° dips, which is controlled by the internal and sliding frictions of the rocks (e.g., Anderson, 1951; Byerlee, 1978; Collettini and Sibson, 2001). However, it is not exceptional that very low-angle normal faults, i.e., at or <30° dips, are observed both in the field and rift basins (e.g., Wernicke et al., 1985; Axen et al., 1990; Axen, 1993; Davis and Lister, 1988; Chiaraluce et al., 2007). Similarly, the major fault F1 in our study area is a large-scale low-angle normal fault developing together with high-angle faults in the upper crust. The mechanics of low-angle normal fault development has been debated for decades, with key questions concerning about whether a given fault initiated at low dip and whether the fault was active at low dip. There are several possible factors leading to occurrence of extensional faults with low dips, mainly including: i) rotation of fault plane from initially high-angle to low-angle (Wernicke and Burchfiel, 1982; Davis 1983; Buck, 1988; Wernicke and Axen, 1988; Axen et al., 1995; Wernicke, 1995), ii) magmatic activity (Lister and Baldwin 1993; Parsons and Thompson, 1993), iii) elevated pore-fluid pressure or presence of low-friction materials in the fault core (Axen, 1992; Rice, 1992; Hayman et al., 2003; Numelin et al., 2007; Collettini et al., 2009a, 2009b), and iv) reactivation of pre-existing thrust faults (Coward et al., 1989; Ghisetti and Vezzani, 1999; Collettini et al., 2006; Bird et al., 2015). Following analysis considers the plausible contribution of those factors.

Previous studies reported several low-angle normal faults associated with post-deformational rotation of initially high-angle faults, such as the Snake Range detachment (Miller et al., 1983), Basin and Range faulting, western Nevada (Proffett, 1977), and Sierra Mazatán core complex in NW Mexico (Wong and Gans, 2008), which were explained by a 'rolling hinge' (e.g., Buck, 1988; Wernicke and Axen, 1988; Axen et al., 1995; Wernicke, 1995; Hamilton, 1988), or 'domino-style' rotation model (e.g., Proffett 1977; Wernicke and Burchfiel, 1982; Davis 1983; Wong and Gans, 2008). The rotation models imply that rotation of initially high-angle fault occurs during or after the initiation of fault plane, so that corresponding footwall rotation and/or stratigraphic truncation is to be observed at the crest of the footwall block. Alternatively, it is likely that a younger half-graben occupies the footwall of the rotated fault owing to relative subsidence created by rotation. In our study area, however, the observations stand in contradiction with the rotation models. Firstly, the top basement in the footwall of fault F1 is sub-horizontal and overlain by a tabular package of post-rift stratigraphy, suggesting that no new half-graben forms in the footwall of fault F1, and that there is no demonstrable rotation of the footwall block during and after the deposition of post-rift stratigraphy (Fig. 6). In addition, no other prominent fault with the same orientation and offset develops in the footwall of fault F1, which is unfavourable for simultaneous rotation of fault blocks. For the same reason, the sub-tabular syn-rift stratigraphy portrayed in the central part of fault F1 also support that the plane of fault F1 undergoes no significant rotation from its active period (Fig. 6b). Secondly, at the southwestern part of fault F1, the syn-rift stratigraphy is featured by a roll-over structure that expands toward the border fault F1, gradually thins and flattens on the crest of the hanging wall block (Fig. 6a). This observation represents syn-depositional structure associated with variation in dip angle of the border fault F1 with depth, i.e., the 'ramp-flat' fault shape, and so these dips may be due to rollover of an independently deforming hanging wall block, rather than a measure of rotation of the fault plane (e.g., Xiao et al., 1991). The top basement and syn-rift stratigraphy in the hanging

wall of the northern part of fault F1 are tilted, but it is more likely related to a localized warped effect at the interaction zone of faults F1 and F2 (Figs. 6c and 7). Finally, the cross-cutting relationship for the high-angle fault F8 and low-angle fault F1 indicates that fault F1 had no strong rotation since it initiated, otherwise fault F8 should be simultaneously rotated to a lower dip (Fig. 9c). Based on the evidences mentioned above, there is a small possibility that the low-angle major fault F1 is an initially high-angle fault that rotates during or after its active period.

Previous studies also investigated the relationship between magmatism and continental extension, supporting that magmatism could cause a significant heterogeneity in the stress regime that drives low-angle faulting, in the way of either rotating the greatest principal stress orientation off vertical or weakening the crust through thermal softening at or near magma intrusion (Parsons and Thompson, 1993; Campbell-Stone et al., 2000). For our study area, thermal events were suggested to accompany with the onset of the South China Sea rift, inducing extensive magmatism that led ~30% of the land area to be made up of extension-related plutons and volcanic rocks (Lai et al., 1996; Sewell et al., 2012), and created the giant NE-trending coastal igneous zone during the Early Cretaceous (e.g., Li, 1999; Zhou and Li, 2000). The majority of the NE-trending structures was linked to the intense phase of volcanic and plutonic activity, including the Tolo Channel fault zone system (Sewell et al., 2000). Based on the previous researches, it is possible that magmatic activity played an effect on the formation of low-angle normal faults during the Late Cretaceous to Early Cenozoic rifting of the South China Sea; however, it is difficult to determine how big the effect is, not to mention that rift-related magmatism is also a characteristic of metamorphic core complex resulting from significant uplift of the footwall of a low-angle fault. Therefore, the effect of magmatism on the local stress field during extension essentially resembles the rotation mechanism of initially high-angle fault as described in the 'rolling-hinge' model, and more specific examination on the temporal and spatial relationship between magmatism and rift-related structures is needed for determining the mechanism of low-angle fault development.

There are also some low-angle extensional faults seem to form or slip with low dips, such as the Whipple-Chemehuevi detachment fault system in the Basin and Range, SE California (Yin and Dunn, 1992). According to previous researches, slip on low-angle normal fault requires some specific circumstances that reduce the frictional strength of the rocks in fault core, including: i) presence of low-friction materials (Hayman et al., 2003; Numelin et al., 2007; Collettini et al., 2009a), ii) elevated pore fluid pressure (Axen, 1992; Rice, 1992), and iii) sub-horizontal weak zone (Yin,1989; Melosh, 1990). Regarding to our study area, the factor of sub-horizontal weak zone can be firstly excluded, because at the rift onset, the basement rocks were mainly composed of granitic plutons with high frictional strength (e.g., Lu et al., 2011; Yi et al., 2012; Sun et al., 2014). In addition, the depth where the low-angle normal fault existed was not deep enough to be affected by an underlying ductile shear zone. Since the presence of low-frictional materials, i.e., phyllosilicates, has been found in the clay gouge of the thrust faults in the Pearl River Delta area (e.g., Nanni et a., 2017), we argue that clay gouge formation may have played an effect on the development of low-angle normal faults. However, it is noteworthy that formation of low-friction clay-rich material and elevated pore fluid pressure occur in unusual conditions within fault core, associated with a low-temperature metasomatic reaction or generation of interior low-permeability zone. As such, fluid-rock diagenesis alters the compositions and mechanical properties of fault zone rocks under specific temperature and pressure conditions within the fault core, rather than the intact

rocks. Therefore, those factors do not directly shed light on initiation of low-angle normal fault in the undeformed rocks, but offer a potential mechanical basis for a pre-existing fault to subsequently move at low dips.

Low-angle normal faults have been observed in the central Apennies, where their origin is suggested to be subduction rollback (Collettini et al., 2006) or collapse of an overthickened accretionary wedge, whereby thrust faults are reactivated as low-angle normal faults (Ghisetti and Vezzani, 1999). Also, reactivation of Caledonian thrust belts by Devonian extensional shear zones was extensively recognized in the northern North Sea, and thought to be responsible for the development of low-angle normal faults or shear zones at <30° dips in the lower crust (e.g., Coward et al., 1989; Bird et al., 2015; Phillips et al., 2016; Fazlikhani et al., 2017). Similarly, we suggest that reactivation of basement thrust fault is the primary cause for the formation of low-angle normal fault in our study area on account of the following proofs. Firstly, we observe a number of pre-existing thrust faults in the basement of the study area, i.e., basement faults BF1-BF6, which are separated and have different deformation manner from cover structures. We therefore interpret them to be originated from the compressional tectonics related to the subduction of the Pacific Ocean Plate under the South China Block. This observation is consistent with the study of Ye et al. (2020), which identified several groups of Mesozoic thrust faults in the basement of the Pearl River Mouth Basin. In addition, some Early Cretaceous, NE- to E-W-striking thrust faults and NE-SW-striking strike-slip faults, e.g., the Tiu Tan Lung Fault and the San Tin Fault, were found in the field outcrops, which are suggested to be of same origin with those in the offshore basins (Nanni et al., 2017). Based on those observations, we argue that there have developed pervasive thrust faults in the basement of the study area, related to the Late Mesozoic compressional event. Secondly, we find some of the rift faults are explicitly associated with reactivation of basement thrust fault. A good example is the low-angle major fault F1, the along-strike extension of which coincides with the intrabasement fault BF6 (Fig. 6), indicating that the low-angle fault F1 initiated by employing a previously existing basement fault plane. In other words, the intrabasement fault BF6 and the low-angle fault F1 are two parts of a basement thrust fault before the rifting, and when the rifting started, one part was employed as the shear plane of the low-angle fault F1, whereas the other part remained inactive and was left over to be the intrabasement fault BF6. That is why the intrabasement fault BF6 overlaps with the extension line of the low-angle fault F1. Another example is the rift fault F3 that merges with the intrabasement fault BF3 at depth. The intrabasement fault BF3 has quite similar dips and seismic reflection features with the lower part of fault F3, as if they were originally one through-going fault, namely the basement thrust fault BF3. We argue that the lower part of basement thrust fault BF3 was employed as the shear plane of fault F3 at the beginning of the rifting, from where fault F3 propagated upwards at a steeper dip. As a result, the upper part of basement thrust fault BF3 remained inactive, and became a residual segment situating in the footwall of fault F3. The two listed examples provide a solid proof that pre-existing basement thrust faults in our study area can reactivate and dominate the normal fault system during later rifting stage, and should be responsible for the formation of low-angle normal faults.

In summary, the most unlikely factor for low-angle fault formation in our study area is late-stage rotation of fault plane from an initial high dip to later low dip, because the syn-rift beds are not significantly rotated during and after its active period. To be noted, we cannot rule out that magmatism during rifting is a possible beneficial factor allowing for low-angle fault development because we have no proofs to exclude it. We argue that clay gouge formation may play an effect on the

development of low-angle normal faults, but cannot be the main factor for the initiation of low-angle fault because clay gouge is commonly localized within the fault core. From this perspective, we suggest that reactivation of pre-existing thrust fault is ranked the primary factor that controls the formation of the low-angle normal faults, and possibly with the help of low-friction materials within the fault core. Therefore, our observations support that the low-angle normal fault bounding the Enping sag was originated from the reactivation of a basement thrust fault forming before the rifting, which is consistent with suggestion of Ye et al. (2018).

6.2 Reactivation mode of basement thrust fault and controlling factors

As mentioned above, the development of low-angle fault F1 results from reactivation of a basement thrust fault, implying that fault evolution in our study area is influenced by pre-existing basement faults. Our focus here is to figure out the variety in reactivation pattern of basement thrust fault. For instance, reactivation of the basement thrust fault BF6 is partial along strike; that is, one part reactivates and generates the low-angle fault F1, while the other part remains as an intrabasement fault being buried by later rift sequences (Fig. 6d). Another example of partial reactivation is the basement thrust fault BF3. Those examples suggest that reactivation of basement thrust fault is not simply reutilizing the pre-existing plane of thrust fault and reversing the slip direction of fault block, but is characterized by partial reactivation in cross-section or map view, with the remnants being left within the basement. Besides, we note that a lot of intrabasement faults have no later activity during the rifting stage. For instance, the intrabasement faults in the hanging wall of major fault F1, i.e., BF1, tips-out at the top basement, which is a sign of no movement after the rift sequences overlie it (Fig. 5a). Also, there are some intrabasement faults in the footwall of fault F4 that terminate below the top basement at the upper tip (Fig. 5c). More cases of unactivated basement thrust faults have been found in the onshore area of the northern South China Sea, where outcrops of basement thrust faults was widely reported (Nanni et al., 2017). Even though full reactivation is not directly observed here, it is likely to occur to the south, e.g., the Baiyun and Liwan sags, because of a higher potential for pre-existing structures to be reactivated at the proximity of rift centre (Wang et al., 2018). Besides, full reactivation of pre-existing fault has been well portrayed in other natural rifts, e.g., the Horda Platform in the northern North Sea (e.g., Bell et al., 2014; Duffy et al., 2015; Phillips et al., 2016; Fazlikhani, et al., 2017), and numerical models investigating multiple phases of rifting (e.g., McClay and White, 1995; Keep and McClay, 1997; Bellahsen and Daniel, 2005; Henza et al., 2010, 2011; Chattopadhyay and Chakra, 2013; Henstra et al., 2015; Deng et al., 2017b, 2018; Zwaan and Schreurs, 2017; Molnar et al., 2019; Maestrelli et al., 2020; Gouiza et al., 2021; Samsu et al., 2021; Wang et al., 2021; Zwaan et al., 2021), from which we can learn lessons.

Based on the observations from the northern South China Sea (e.g., Nanni et al., 2017; Ye et al., 2018, 2020; Zhou et al., 2019), other natural rift basins (e.g., Morley, 2004, 2007; Bell et al., 2014; Duffy et al., 2015; Phillips et al., 2016; Fazlikhani et al., 2017), and numerical models (e.g., Deng et al., 2017b, 2018), reactivation of a basement thrust fault can be classified into three modes: i) no reactivation, ii) partial reactivation, and iii) full reactivation. For a better understanding of the variety in the reactivation mode, we develop a conceptual model highlighting the key characteristics and interaction style with adjacent normal faults (Fig. 11). In details, unactivated basement thrust fault keeps as blind fault beneath the top basement and is cross-

cut by newly-formed high-angle faults, which provides a solid evidence for the presence of pre-existing basement structures prior to rifting (Fig. 11a). In contrast, partly or fully reactivated basement thrust fault develops into low-angle normal fault under favourable conditions during later rifting stage, and influence the geometry of newly-formed high-angle faults. For example, a partly reactivated basement thrust fault slips at low dips and becomes a major fault, with its inactive portion being preserved as a hint of partial reactivation, and the reactivated portion being featured by merging and abutting interactions with newly-formed high-angle normal faults (Fig. 11b). Furthermore, a fully reactivated basement thrust fault has similar fault interactions with partly reactivated one; however, it is prominent that the resultant fault network appears geometrically different (Fig. 11c). In details, fully reactivated basement thrust fault has a through-going fault trace with a bigger length and displacement, whereas partly reactivated one consists of a few numbers of fault segments with smaller length and displacement. As a whole, the fault network comprising reactivated basement thrust faults and new normal faults become more complex with an increasing reactivation extent, because of a larger possibility of fault interactions. This conceptual model can be largely applicable to the rift setting with pre-existing thrust faults.

We also observe that unactivated basement thrust faults are more pervasive than reactivated ones, as found in the hanging-wall and footwall of the major fault F1 (Figs. 5 and 6), where reactivation of basement thrust faults is selective. According to previous studies, reactivation of a pre-existing fault mainly depends on fault strength (e.g., Etheridge, 1986; Ranalli & Yin, 1990; Dubois et al., 2002; Bellahsen & Daniel, 2005), state of stress in three dimensions (e.g., Sibson, 1985; Ranalli & Yin, 1990), strain magnitude (e.g., Henza et al., 2010, 2011; Wang et al., 2021;), and extension direction (e.g., Bonini et al., 1997; Keep & McClay, 1997; Henza et al., 2010, 2011; Chattopadhyay and Chakra, 2013; Zwaan and Schreurs, 2017; Deng et al., 2017b, 2018; Molnar et al., 2019; Maestrelli et al., 2020; Samsu et al., 2021). Regarding to our case, the different reactivation modes of basement thrust faults are not likely to be related to different fault strength, because they are of same age and origin related to the Middle Jurassic to Early Cretaceous compressional event, so that they should have similar strength. Using scaled analogue models, Henza et al. (2010, 2011) observed that strain magnitude could dominate the geometries of the final fault network, and the reactivation of first-phase faults has a positive correlation with the angle between the extension directions. The variety in reactivation mode coexists where pre-existing faults have various orientations (e.g., Claringbould et al., 2017), but in our case, there is no direct correlation between fault orientation and reactivation mode, because unactivated and reactivated NE-SW-striking basement thrust faults are both observed. Since strain magnitude in one rift system increases from margin to centre, we suggest that the reactivation potential of basement thrust faults increases in that direction as well. In addition, Phillips et al. (2016) suggest that selective reactivation of pre-existing structures is greatly dependent on their scale and dip, with large-scale, steeply-dipping structures preferentially reactivated and smaller, shallowly-dipping structures cross-cut. Another possible reason is the strain shadow zone encircling reactivated thrust faults. We argue that the strain is likely to be localized on a few reactivated major faults, i.e., the major fault F1 that has a big length and displacement, causing strain shadow zone to form in their vicinity. If so, other small basement faults in the strain shadow zone are prevented from reactivation. This is consistent with the suggestion made by Ackermann and Schlishce (1997) that a stress-reduction shadow naturally forms around active master faults, where the nucleation of smaller faults is retarded. Therefore, a combination of

overall strain distribution, scale of pre-existing faults and strain shadow zone surrounding reactivated ones leads to a limited number of fault reactivation in rift basin underlain by pervasive basement thrust faults.

6.3 Impacts of basement thrust fault on normal fault development

The impact of pre-existing structure or fault on the geometry and evolution of normal fault mainly involves altering fault density (e.g., Willemse et al., 1996; Ackermann and Schlische, 1997; Gupta and Scholz, 2000; Cowie and Roberts, 2001; Soliva et al., 2006), strike and dip (e.g., Morley et al. 2004, 2007; Henza et al., 2010, 2011; Chattopadhyay and Chakra, 2013; Zwaan and Schreurs, 2017; Deng et al., 2017b, 2018; Molnar et al., 2019; Maestrelli et al., 2020; Samsu et al., 2021), displacement (e.g., Duffy et al., 2015; Deng et al., 2017b, 2018), and offering nucleation sites to neighbouring new faults (Morley et al., 2004, 2007; Phillips et al., 2016; Deng et al., 2017b). The fault development in our study area is also influenced by the reactivation of pre-existing basement faults. For instance, fault density is relatively low in the hanging wall of the major fault F1, implying the presence of strain shadow zone around fault F1. In addition, the geometry of faults F2 and F5 reflects the effect of reactivated fault on the dip and displacement of new faults. However, the particularity of our study area is that the low-angle normal fault F1 associated with reactivated basement thrust fault developed at broadly the same time and location with the high-angle ones, and played a dominant role in fault evolution. Such importance of low-angle fault on normal fault growth and rift development has been emphasized in the Basin and Range (e.g., Hamilton, 1988; Axen et al., 1990; Campbell-Stone et al., 2000) and the northern North Sea Rift (e.g., Phillips et al., 2016; Fazlikhani et al., 2017). Now we focus on how the reactivation of basement thrust fault affects the growth of newly-formed faults.

The first impact is that reactivated basement thrust fault affects the dip of overlying new faults, represented by the 'merging fault' that initiates at high dips within the hanging wall of the low-angle major fault F1 and has an obvious decrease in dip as propagating downward to the slipping plane of fault F1 (Fig. 9a). Such effect indicates that the dip of rift-related faults may be influenced by the underlying low-angle major fault. This observation can be explained by the anisotropic mechanics of the rocks adjacent to the major fault F1, which underwent a long-term activity from the Mesozoic thrust fault to the Cenozoic extensional fault, generating a deformation zone full of small-scale interweaved fractures and/or low-friction materials in the fault rocks (e.g., Scheiber et al., 2015). As such, normal fault can slip at a low dip given that the rocks are sufficiently weakened. In addition, this weakening effect lays a foundation for the downdip amalgamation of faults F1 and F2, which results in abandonment of the upper part of fault F1 after linkage. This effect of basement structure on the dip of later rift faults is consistent with the suggestion made by Ring (1994) that Proterozoic basement structures represented the basic anisotropy influencing pre-Cenozoic rifts and also the Cenozoic Malawi rift, and echoes that low-friction materials forming within fault zone can act to weaken a pre-existing fault surface, and thus permit it to slip at lower dips (Haines et al., 2014). Another impact is that reactivated basement thrust fault offers nucleation sites for normal faults. For instance, the position of throw maximum of fault F4 suggests that fault F4 initiates at the upper tip of the low-angle fault F1, from where it propagates radially as a new high-angle fault plane (Fig. 9b). In addition, the domino faults have similar growth pattern; that is, they nucleate at the plane of low-angle fault F1, and then propagate upwards from it at higher dips, indicated by their throw maximum at the intersection

with the low-angle fault F1(Fig. 9c). This impact on nucleation of new faults can also be explained by the local weaknesses/fractures within the deformation zone of the major fault F1. Based on the two examples, we argue that there is strain localization on the weaknesses or fractures, which are employed as nucleation sites of future faults. Fazlikhani et al. (2017) described similar fault nucleation on low-angle shear zone in the northern North Sea, and suggested that basement shear zone acted as pre-existing weakness for providing nucleation sites of future faults, which is consistent with our observation.

The above two impacts are suggestive of two evolution models of a reactivated pre-existing fault and nearby new faults during rifting: i) the 'decoupled model' in which reactivated pre-existing fault and nearby new faults are initially isolated at different levels, followed by later propagation and final linkage to form a connect fault system (Fig. 12a; Childs et al., 1996; Schöpfer et al., 2006; Jackson & Rotevatn, 2013); and ii) the 'coupled model' in which new faults nucleate at pre-existing fault and grow as kinematically related components of a fault array, where pre-existing fault serves as nucleation sites of new faults (Fig. 12b; e.g., Childs et al. 1995, 1996; Walsh et al., 2002, 2003; Morley et al., 2004; Baudon and Cartwright, 2008). For the case of faults F1 and F2, we find that fault F2 evolves from an initially isolated fault segment in the hanging wall of the low-angle major fault F1 to ultimate merging into fault F1, similar to the 'decoupled model'. Such decoupling evolution is also described in numerical models, claiming that new faults independently initiate in the succession overlying the pre-existing fault if it is thick enough (e.g., Deng et al., 2018). As for our case, the reason that the reactivated and new faults develop in an initially decoupled pattern is possibly related to the thick thrust belts in the upper part of the basement, so that new faults need to accumulate sufficient strain for cutting off the thick basement rocks before reaching the reactivated fault. In comparison, the domino faults are both geometrically and kinematically linked to the major fault F1 in their early history and then grow upward as a connected fault system. Such 'coupled model' possesses the general conception that pre-existing fault is a weakness being favourable for nucleation of future faults. We suggest that the syn-rift stratigraphic cover where the domino faults form is much thinner and weaker than the underlying basement rock, so that the domino faults can cut through the syn-rift stratigraphy with a small amount of strain. Summarizing, the two different growth models imply that reactivated basement thrust fault exerts a significant effect on the geometry and growth of new faults within the hanging wall. Also, such difference reflects that the growth pattern of the reactivated fault and nearby new faults is closely related to the hanging-wall rock strength. Based on the above analysis, we provide a preliminary case study for identifying the relationship between pre-existing thrust faults and new rift faults, and improving the understanding of fault evolution in rift basin affected by pre-existing thrusting structures, which has been paid less attention in previous researches.

6.4 Implications for tectonic evolution of the northern South China Sea

A variety of models have been proposed for explicating the opening mechanism of the South China Sea, but most famous are: i) the 'pull-apart model' that the opening is attributed to southeast extrusion of the Indochina Block driven by the collision between India and Asia (Tapponnier et al., 1982, 1990, 2001; Briais et al., 1993; Leloup et al., 1995, 2001; Gilley et al., 2003); and ii) the 'slab-pull model' that the opening results from slab rollback and retreat of the paleo-Pacific Plate linked with northward subduction of a proto-South China Sea at the north Borneo Trench (Taylor and Hayes, 1980, 1983; Lee and Lawver,

1995; Rangin et al., 1995; Hall, 2002; Morley, 2002, 2012). Both models raise a general hypothesis that the South China Sea underwent a transition from convergent Andean-type continental margin to divergent Western Pacific-type margin during the Late Mesozoic (Holloway, 1982; Taylor and Hayes, 1983; Li and Li, 2007; Li et al., 2012; Shi and Li, 2012). Our study supports that the South China Sea rift is built on the inhomogeneous basement with a series of pre-existing thrust faults that stem from an earlier compression/subduction tectonics. Apart from our study area, the neighbouring sags within the Pearl River Mouth Basin and adjacent rift basins, e.g., the Zhu I Depression (Ye et al., 2020), Chaoshan Depression (Li et al., 2008; P. Yan et al., 2014), the Qingdongnan basin (Hu et al., 2013), the Taixinan basin (Li et al., 2007), and even the Nansha Trough at the southern margin of the South China Sea (Yan and Liu, 2004; Wang et al., 2016), also contain a number of pre-existing NE-SW- to NEE-SWW-trending and nearly E-W-trending basement fabrics that are believed to affect the development of the rift-related faults and basins during the Late Cretaceous to Cenozoic rifting (Lister et al., 1986; Zhou et al., 1995; Zhu and Jiang, 1998; Sun et al., 2009, 2010; Hu et al., 2013; Ye et al., 2018, 2020). In addition, some NE-SW- and E-W-trending thrust faults and strike-slip faults of the Jurassic to Early Cretaceous have been found in the field outcrops of the Pearl River Delta area, at the northern margin of the South China Sea, and some of them were reactivated by Cenozoic extensional structures (Nanni et al., 2017). Based on the above-mentioned researches, we agree that a Mesozoic subduction zone have developed along the northern margin of the South China Sea, or further south along the Dangerous Ground and North Palawan, associated with the Jurassic-Cretaceous Yanshanian movement due to subduction of the paleo-Pacific Plate beneath the South China Block (Faure et al., 1996; Ren et al., 2002; Shu et al., 2006; Zhou et al., 2006). Our study is consistent with previous studies about the origin of basement thrust faults, and supports that the formation of the South China Sea rift system and reverse reactivation of basement thrust faults are mainly governed by the dynamic transition from compressional to extensional setting. Therefore, we argue that the tectonic evolution of the northern South China Sea rift, especially the area close to the Mesozoic subduction zone, should be greatly influenced by quite a few groups of basement-rooted thrusting structures, and so examining their spatial and temporal evolution is of vital importance for understanding the structural styles of subsequent rift and fault system.

Integrating the observations from our study and neighbouring areas, we construct a conceptual model illustrating how the presence of intrabasement thrust faults influences the geometry and evolution of subsequent rift system (Fig. 13). Firstly, reactivated basement thrust fault controls the location and geometry of rift boundary fault (Fig. 13b-c). In specific, fault F1 originated from the reactivated basement thrust fault grows into the major fault bounding a wide and shallow half-graben owing to its gentler dip (Fig. 6). This point is consistent with Walsh et al. (2002), which proposed that reactivation of pre-existing fault is characterized by 'near-constant' growth model that reactivated basement fault rapidly obtains its near-maximum length and becomes the major fault, followed by a long period of displacement accrual. As such, strain is distributed over a wide and shallow basin area in the hanging wall of the low-angle boundary fault, leading to a more gently-dipping landform from rift margin to depocenter (Fig. 13b).We therefore argue that rift system affected by underlying basement thrust faults will generate specific fault geometry, basin topography and depositional system that differ from those established models of rift evolution, because syn-rift stratigraphic sequence is sensitive to a change in the basin paleotopography (e.g., Gawthorpe

& Leeder, 2000; Cowie et al., 2006). This point will play an important role in subsequent investigation of basin sedimentology and petroleum geology, so bearing it in mind is essential for geologists to predict sediment infilling pattern, facies and hydrocarbon reservoirs in those rifted basins. Secondly, there will be a decreasing trend in reactivation potential of basement thrust faults from rift centre to rift margin, due to a decrease in the strain magnitude toward rift margin (e.g., Cowie et al., 2015). In details, without considering other aspects, there will be more chances for reactivation of basement thrust faults near rift centre, whereas at rift margin, basement thrust faults are prone to remain unactivated (Fig. 13b). Such a scenario provides a template for future fault and basin structure in rift affected by underlying basement structures. Nearby rift centre, newly-formed faults either develop as minor structures in the space between major reactivated faults in order to adjust interior deformation of fault blocks, or merge into the slipping plane of reactivated faults to form a connected fault system (Fig. 13c). In comparison, at the rift margin where basement thrust faults hardly reactivate and affect new fault development, the fault network should be featured by a group of evenly spaced, sub-parallel new faults offsetting pre-existing basement thrust faults, which is similar to the rift development within homogeneous crust (e.g., Gupta et al., 1998; Cowie et al., 2000; Gawthorpe and Leeder, 2000). Summarizing, we argue that the tectonic evolution of the northern South China Sea is greatly influenced by the presence of intrabasement thrust faults, in the way of controlling the location and degree of faulting that occurs during rifting, and the overall basin structures and paleotopography.

7 Conclusions

This study aims to investigate how basement thrust fault evolves and influences the development of rift system and normal fault during subsequent rifting, and what enlightenments that influence has on the subsequent basin structure and syn-rift stratigraphic sequence. Our observations suggest that basement thrust fault could reactivate and slip as low-angle normal fault during later rifting, and then exert significant effects on the nucleation, dip and displacement of nearby new faults, resulting in several styles of fault interactions, e.g., merging, abutting and crosscutting. Key conclusions obtained from this investigation include:

(1) Basement thrust faults were pervasively distributed in the South China Sea area before the Late Cretaceous to Early Cenozoic rifting phase, and their later reactivation is the primary cause for the development of low-angle normal fault during rifting, possibly with the assistance of low-friction materials in the fault core.

(2) Reactivation mode of basement thrust fault includes full, partial and no reactivation, depending on overall strain distribution across rift, scale of basement thrust fault and strain shadow zone surrounding reactivated ones.

(3) Reactivated basement thrust fault influences the nucleation, dip and displacement of nearby new faults, causing them to nucleate at or merge into the fault plane downwards.

(4) Rift structure affected by underlying basement thrust structures are characterized by shallowly-dipping basin topography, and formation of shallower and wider basin depocenter for syn-rift sediment infill, which is crucial for further investigation of basin sedimentology and petroleum geology.

Summarizing, the tectonic evolution of the northern South China Sea rift, especially the area close to the Mesozoic subduction zone, is greatly affected by quite a few groups of basement-rooted thrusting structures, and so examining their spatial and temporal evolution is of vital importance for understanding the structural styles of the subsequent rift and fault system.

Acknowledgements

This study is supported by Shenzhen Branch of CNOOC of China (Project No. 2017-RFPSZ-0613), China Postdoctoral Science Foundation (No. 234012000002), research fund from the State Key Laboratory of Continental Dynamics and Department of Geology, Northwest University (No. 111110005) and National Natural Science Foundation of China (No. 42002124). We appreciate the thoughtful discussions and suggestions from Ge zhiyuan at China University of Petroleum (Beijing), and thank Wang tianbao for his support and assistance in data collection.

References

Ackermann, R. V., & Schlische, R. W. (1997). Anticlustering of small normal faults around larger faults. Geology, 25(12), 1127-1130.

Anderson, E.M., 1951. The Dynamics of Faulting. Olivier and Boyd, Edinburgh. 206pp.

Axen, G. J. (1988). The geometry of planar domino-style normal faults above a dipping basal detachment. Journal of Structural Geology, 10(4), 405-411.

Axen, G. J., 1993. Ramp-flat detachment faulting and low-angle normal reactivation of the Tule Springs thrust, southern Nevada, Geol. Soc. Am. Bull., 105, 1076-1090.

Axen, G. J., B. Wernicke, M. J. Skelly, and W. J. Taylor, 1990. Mesozoic and Cenozoic tectonics of the Sevier thrust belt in the Virgin River Valley area, southern Nevada, in Basin and Range Extensional Tectonics Near the Latitude of Las Vegas Nevada, edited by B. Wernicke, Mem. Geol. Soc. Am., 176, 123-153.

Axen, G. J., J. M. Bartley, and J. Selverstone. 1995. Structural expression of a rolling hinge in the footwall of the Brenner Line normal fault, eastern Alps. Tectonics 14:1380-1392.

Axen, G., 1992. Pore pressure, stress increase and fault weakening in low-angle normal faulting. J. Geophys. Res. B, Solid Earth Planets 97, 8979-8991.

Badley, M., Price, J., Dahl, C.R., Agdestein, T., 1988. The structural evolution of the northern Viking Graben and its bearing upon extensional modes of basin formation. J. Geol. Soc. 145, 455-472.

Baudon, C., Cartwright, J., 2008. The kinematics of reactivation of normal faults using high resolution throw mapping. J. Struct. Geol. 30, 1072-1084.

Bell, R.E., Jackson, C.A.L., Whipp, P.S., Clements, B., 2014. Strain migration during multiphase extension: observations from the northern North Sea. Tectonics 33, 1936-1963.

Bellahsen, N., & Daniel, J. M. (2005). Fault reactivation control on normal fault growth: An experimental study. Journal of Structural Geology, 27(4), 769-780.

Bellahsen, N., Fournier, M., d'Acremont, E., Leroy, S., Daniel, J., 2006. Fault reactivation and rift localization: Northeastern Gulf of Aden margin. Tectonics 25.

Bird, P. C., J. A. Cartwright, and T. L. Davies (2015), Basement reactivation in the development of rift basins: An example of reactivated Caledonide structures in the west Orkney Basin, J. Geol. Soc. Lond., 172(1), 77-85.

Bonini, M., Souriot, T., Boccaletti, M., & Brun, J. P. (1997). Successive orthogonal and oblique extension episodes in a rift zone: Laboratory experiments with application to the Ethiopian rift. Tectonics, 16(2), 347-362.

Bonini, L., Basili, R., Burrato, P., Cannelli, V., Fracassi, U., Maesano, F.E., Melini, D., Tarabusi, G., Tiberti, M.M., Vannoli, P., Valensise, G., 2019. Testing different tectonic models for the source of the Mw 6.5, 30 October 2016, Norcia earthquake (central Italy): a youthful normal fault, or negative inversion of an old thrust? Tectonics 38, 990–1017. https://doi.org/10.1029/2018TC005185.

Bonini, L., Basili, R., Toscani, G., Burrato, P., Seno, S., & Valensise, G. (2015). The role of pre-existing discontinuities in the development of extensional faults: an analog modeling perspective. Journal of structural geology, 74, 145-158.

Briais, A., Patriat, P., Tapponnier, P., 1993. Updated interpretation of magnetic anomalies and sea-floor spreading stages in the South China Sea – implications for the Tertiary tectonics of Southeast-Asia. J. Geophys. Res. – Solid Earth 98, 6299-6328.

Buck, W., 1988. Flexural rotation of normal faults. Tectonics7, 959-974.

Byerlee, J., 1978. Friction of rocks. Pure Appl. Geophys.116, 615-626.

Campbell-Stone, E., John, B. E., Foster, D. A., Geissman, J. W., and Livaccari, R. F. (2000), Mechanisms for accommodation of Miocene extension: Low-angle normal faulting, magmatism, and secondary breakaway faulting in the southern Sacramento Mountains, southeastern California, Tectonics, 19(3), 566-587, doi:10.1029/1999TC001133.

Cartwright, J., Bouroullec, R., James, D., Johnson, H., 1998. Polycyclic motion history of some Gulf Coast growth faults from high-resolution displacement analysis. Geology 26, 819-822.

Cartwright, J., Trudgill, B. D., & Mansfield, C. S. (1995). Fault growth and segment linkage: An explanation for scatter in maximum displacement and trace length data from the Canyonlands grabens of Se Utah. Journal of Structural Geology, 17(9), 1319-1326.

Charvet, J., Lapierre, H., Yu, Y., 1994. Geodynamic significance of the Mesozoic volcanism of southeastern China. J. SE Asian Earth Sci. 9 (4), 387-396.

Chattopadhyay, A., and Chakra, M. (2013). Influence of pre-existing pervasive fabrics on fault patterns during orthogonal and oblique rifting: An experimental approach. Marine and Petroleum Geology 39(1), 74-91. doi: 10.1016/j.marpetgeo.2012.09.009.

Chiaraluce, L., C. Chiarabba, C. Collettini, D. Piccinini, and M. Cocco (2007), Architecture and mechanics of an active low angle normal fault: Alto Tiberina Fault, northern Apennines, Italy, J. Geophys. Res., 112, B10310, doi:10.1029/2007JB005015.

Childs, C., Nicol, A., Walsh, J.J., Watterson, J., 1996. Growth of vertically segmented normal faults. Journal of Structural Geology 18, 1389-1397.

Childs, C., Watterson, J., Walsh, J.J., 1995. Fault overlap zones within developing normal fault systems. J. Geol. Soc. 152 (3), 535-549.

Claringbould, J. S. , Bell, R. E. , Jackson, A. L. , Gawthorpe, R. L. , & Odinsen, T. . (2017). Pre-existing normal faults have limited control on the rift geometry of the northern north sea. Earth and Planetary Science Letters, 475, 190-206.

Collettini, C., De Paola, N., Holdsworth, R.E., and Barchi, M.R., 2006, The development and behaviour of low-angle normal faults during Cenozoic asymmetric extension in the Northern Apennines, Italy: Journal of Structural Geology, v. 28, p. 333-352, https://doi.org/10.1016/j.jsg.2005.10.003.

Collettini, C., Niemeijer, A., Viti, C., Marone, C., 2009a. Fault zone fabric and fault weakness. Nature 462, 907-910. http://dx.doi.org/10.1038/nature08585.

Collettini, C., Sibson, R., 2001. Normal faults, normal friction? Geology29, 927-930.

Collettini, C., Viti, C., Smith, S., Holdsworth, R., 2009b. The development of inter-connected talc networks and weakening of continental low-angle normal faults. Geology 37, 567-570.

Corti, G. (2009). Continental rift evolution: From rift initiation to incipient break-up in the Main Ethiopian Rift, East Africa. Earth Science Reviews, 96(1-2), 1-53.

Coward, M. P., M. A. Enfield, and M. W. Fischer (1989), Devonian basins of northern Scotland: Extension and inversion related to late Caledonian—Variscan tectonics, in Inversion Tectonics, edited by M. A. Cooper and G. D. Williams, Geol. Soc. London Spec. Publ., 44, 275-308.

Cowie, P. A., Underhill, J. R., MD Behn, Jian, L., & Gill, C. E. (2015). Spatio-temporal evolution of strain accumulation derived from multi-scale observations of late jurassic rifting in the northern north sea: a critical test of models for lithospheric extension. Earth & Planetary Science Letters, 234(3-4), 401-419.

Cowie, P., Attal, M., Tucker, G.E., Whittaker, A.C., Naylor, M., Ganas, A. and Roberts, G.P. (2006), Investigating the surface process response to fault interaction and linkage using a numerical modelling approach. Basin Research, 18: 231-266. https://doi.org/10.1111/j.1365-2117.2006.00298.x.

Cowie, P., Roberts, G.P., 2001. Constraining slip rates and spacings for active normal faults. J. Struct. Geol. 23, 1901-1915.

Cowie, P.A., Gupta, S., Dawers, N.H., 2000. Implications of fault array evolution for synrift depocetre development: insights from a numerical fault growth model. Basin Res. 12, 241-261.

Davis, G. A., and G. S. Lister, 1988. Detachment faulting in continental extension: Perspectives from the southwestern U.S. Cordillera, Spec. Pap. Geol. Soc. Am., 218, 133-159.

Davis, G. H. 1983. Shear-zone model for the origin of metamorphic core complexes. Geology 11:342-347.

Dawers, N. H., & Anders, M. H. (1995). Displacement-length scaling and fault linkage. Journal of Structural Geology, 17(5), 607-614.

Del Ventisette, C., Bonini, M., Maestrelli, D., Sani, F., Iavarone, E., & Montanari, D. (2021). 3D-thrust fault pattern control on negative inversion: An analogue modelling perspective on central Italy. Journal of Structural Geology, 143, 104254. https://doi.org/10.1016/j.jsg.2020.104254

Deng, C. , Gawthorpe, R. L. , Fossen, H. , & Finch, E. . (2018). How does the orientation of a preexisting basement weakness influence fault development during renewed rifting? insights from three-dimensional discrete element modeling. Tectonics, 37(7-8), 2221-2242.

Deng, C., Fossen, H., Gawthorpe, R. L., Rotevatn, A., Jackson, A. L., & Fazlikhani, H. (2017a). Influence of fault reactivation during multiphase rifting: The Oseberg area, northern North Sea rift. Marine and Petroleum Geology, 86, 1252-1272.

Deng, C., Gawthorpe, R. L., Finch, E., & Fossen, H. (2017b). Influence of a pre-existing basement weakness on normal fault growth during oblique extension: Insights from discrete element modeling. Journal of Structural Geology, 105, 44-61.

Dubois, A., Odonne, F., Massonnat, G., Lebourg, T., & Fabre, R. (2002). Analogue modelling of fault reactivation: Tectonic inversion and oblique remobilisation of grabens. Journal of Structural Geology, 24(11), 1741-1752.

Duffy, O. B., Bell, R. E., Jackson, C. A., Gawthorpe, R. L., & Whipp, P. S. (2015). Fault growth and interactions in a multiphase rift fault network: Horda Platform, Norwegian North Sea. Journal of Structural Geology, 80, 99-119.

Etheridge, M. A. (1986). On the reactivation of extensional fault systems. Philosophical Transactions of the Royal Society of London. Series A, Mathematical and Physical Sciences, 317(1539), 179-194.

Færseth, R. (1996). Interaction of Permo-Triassic and Jurassic extensional fault-blocks during the development of the northern North Sea. Journal of the Geological Society, 153(6), 931-944.

Færseth, R. B., Knudsen, B. E., Liljedahl, T., Midbøe, P. S., & Søderstrøm, B. (1997). Oblique rifting and sequential faulting in the Jurassic development of the northern North Sea. Journal of Structural Geology, 19(10), 1285-1302.

Faure, M., Sun, Y., Shu, L., Monie, P., Charvet, J., 1996. Extensional tectonics within a subduction-type orogen. The case study of the Wugongshan dome (Jiangxi Province, southeastern China). Tectonophysics 263, 77-106.

Fazlikhani, H., Fossen, H., Gawthorpe, R. L., Faleide, J. I., & Bell, R. E. (2017). Basement structure and its influence on the structural configuration of the northern North Sea rift. Tectonics, 36, 1151-1177. https://doi.org/10.1002/2017TC004514

Frankowicz, E., McClay, K., 2010. Extensional fault segmentation and linkages, Bonaparte Basin, outer North west shelf, Australia. AAPG Bull. 94, 977-1010.

Gawthorpe, R.L. and Leeder, M.R. (2000), Tectono-sedimentary evolution of active extensional basins. Basin Research, 12: 195-218. https://doi.org/10.1111/j.1365-2117.2000.00121.x.

Ghisetti, F., and Vezzani, L., 1999, Depth and modes of Pliocene–Pleistocene crustal extension of the Apennines (Italy): Terra Nova, v.11, p.67-72, https://doi.org/10.1046/j.1365-3121.1999.00227.x.

Gilley, L.D., Harrison, T.M., Leloup, P.H., Ryerson, F.J., Lovera, O.M., Wang, J.H., 2003. Direct dating of left-lateral deformation along the Red River shear zone, China and Vietnam. J. Geophys. Res. Solid Earth 108. http://dx.doi.org/10.1029/2001JB001726.

Gouiza, M., & Naliboff, J. (2021). Rheological inheritance controls the formation of segmented rifted margins in cratonic lithosphere. Nature Communications, 12(1), 1-9. https://doi.org/10.1038/s41467-021-24945-5

Gupta, A., Scholz, C.H., 2000. A model of normal fault interaction based on observations and theory. J. Struct. Geol. 22, 865-879.

Gupta, S., Cowie, P.A., Dawers, N.H., Underhill, J.R., 1998. A mechanism to explain rift-basin subsidence and stratigraphic patterns through fault-array evolution. Geology 26, 595-598.

Haines, S., Marone, C., Saffer, D., 2014. Frictional properties of low-angle normal fault gouges and implications for low-angle normal fault slip. Earth & Planetary Science Letters. 408, 57-65.

Hall, R., 2002. Cenozoic geological and plate tectonic evolution of SE Asia and the SW Pacific: computer-based reconstructions, model and animations. J. Asian Earth Sci. 20, 353-431.

Hamilton, W., 1988. Detachment faulting in the Death Valley region, California and Nevada, U.S. Geol. Surv. Bull., 1790, 763-771.

Hayman, N., Knott, J., Cowan, D.S., Nemser, E., Sarna-Wojcicki, A., 2003. Quaternary low-angle slip on detachment faults in Death Valley, California. Geology31, 343-346.

Henstra, G.A., Rotevatn, A., Gawthorpe, R.L., Ravnås, R., 2015. Evolution of a major segmented normal fault during multiphase rifting: the origin of plan-view zigzag geometry. J. Struct. Geol. 74, 45–63. https://doi.org/10.1016/j.jsg.2015.02.005.

Henza, A. A., Withjack, M. O., & Schlische, R. W. (2010). Normal-fault development during two phases of non-coaxial extension: An experimental study. Journal of Structural Geology, 32(11), 1656-1667.

Henza, A. A., Withjack, M. O., & Schlische, R. W. (2011). How do the properties of a pre-existing normal-fault population influence fault development during a subsequent phase of extension? Journal of Structural Geology, 33(9), 1312-1324.

Holloway, N.H., 1982. North Palawan block, Philippines—its relation to Asian mainland and role in evolution of South China Sea. AAPG Bull. 66 (9), 1355-1383.

Hu, B., Wang, L., Yan, W., Liu, S., Cai, D., & Zhang, G., et al. (2013). The tectonic evolution of the qiongdongnan basin in the northern margin of the south china sea. Journal of Asian Earth Sciences, 77(nov.15), 163-182.

Jackson, C. A.-L., & Rotevatn, A. (2013). 3D seismic analysis of the structure and evolution of a salt-influenced normal fault zone: A test of competing fault growth models. Journal of Structural Geology, 54, 215-234.

Keep, M., & McClay, K. (1997). Analogue modelling of multiphase rift systems. Tectonophysics, 273(3–4), 239-270.

Lai, K., Campbell, S.D.G., Shaw, R., 1996. Geology of the Northeastern New Territories: Hong Kong Geological Survey Memoir No. 5. Geotechnical Engineering Office, Hong Kong, p. 143.

Le Turdu, C., Tiercelin, J.-J., Richert, J.-P., Rolet, J., Xavier, X.-P., Renaut, R. W., et al. (1999). Influence of pre-existing oblique discontinuities on the geometry and evolution of extensional fault patterns: Evidence from the Kenya rift using SPOT imagery. In C. K. Morley (Ed.), Geoscience of rift systems—Evolution of East Africa (Vol. 44, pp. 173-191). Tulsa, OK: American Association of Petroleum Geologists Studies in Geology.

Lee, T.Y., Lawver, L.A., 1995. Cenozoic plate reconstructions of Southeast Asia. Tectonophysics 251, 85-138.

Leloup, P.H., Arnaud, N., Lacassin, R., Kienast, J.R., Harrison, T.M., Trong, T.T.P., Replumaz, A., Tapponnier, P., 2001. New constraints on the structure, thermochronology, and timing of the Ailao Shan-Red River shear zone, SE Asia. J. Geophys. Res. – Solid Earth 106, 6683-6732.

Leloup, P.H., Lacassin, R., Tapponnier, P., Scharer, U., Zhong, D.L., Liu, X.H., Zhang, L.S., Ji, S.C., Trinh, P.T., 1995. The Ailao Shan-Red River shear zone (Yunnan, China), Tertiary transform boundary of Indochina. Tectonophysics 251, 3-84.

Lepvrier, C., Fournier, M., Bérard, T., Roger, J., 2002. Cenozoic extension in coastal Dhofar (southern Oman): implications on the oblique rifting of the Gulf of Aden. Tectonophysics 357, 279-293.

Lezzar, K. E., Tiercelin, J. J., Turdu, C. L., Cohen, A. S., Reynolds, D. J., Gall, B. L., et al. (2002). Control of normal fault interaction of major Neogene sedimentary depocenters, Lake Tanganyika, East African rift. AAPG Bulletin, 86(6), 1027-1059.

Li, C.F., Zhou, Z.Y., Hao, H.J., Chen, H.J., Wang, J.L., Chen, B., Wu, J.S., 2008. Late Mesozoic tectonic structure and evolution along the present-day northeastern South China Sea continental margin. J. Asian Earth Sci. 31 (4), 546-561.

Li, C.F., Zhou, Z.Y., Li, J.B., Hao, H.J., Geng, J.H., 2007. Structures of the northeasternmost South China Sea continental margin and ocean basin: geophysical constraints and tectonic implications. Mar. Geophys. Res. 28 (1), 59-79.

Li, J., Zhang, Y., Dong, S., Johnston, S.T., 2014. Cretaceous tectonic evolution of south china: a preliminary synthesis. Earth Sci. Rev. 134, 98-136.

Li, P.L., 1993. Cenozoic Tectonic Movement in the Pearl River Mouth Basin. China Offshore Oil Gas (Geol.) 7 (6), 11-17 (in Chinese with English abstract).

Li, P.L., Liang, H.X., Dai, Y.D., Lin, H.M., 1999. Origin and tectonic setting of the Yanshanian igneous rocks in the Pearl River Mouth basin. Guangdong Geol. 14 (1), 1-8 (in Chinese with English Abstract).

Li, X., 1999. Cretaceous Magmatism and Lithosphere Extension in South China: The Geochronology and Geochemistry Constraints. Institute of Geochemistry, Chinese Academy of Sciences. Resource Environment and Sustaining Development. 2647275.

Li, X.H., 2000. Cretaceous magmatism and lithospheric extension in Southeast China. J. Asian Earth Sci. 18 (3), 293-305.

Li, Z., Qiu, J.S., Yang, X.M., 2014. A review of the geochronology and geochemistry of Late Yanshanian (Cretaceous) plutons along the Fujian coastal area of southeastern China: implications for magma evolution related to slab break-off and roll-back in the Cretaceous. Earth Sci. Rev. 128 (1), 232-248.

Li, Z.H., Li, X.H., 2007. Formation of the 1300-km-wide intracontinental orogen and postorogenic magmatic province in Mesozoic South China: a flat-slab subduction model. Geology 35 (2), 179-182.

Li, Z.X., Li, X.H., Chung, S.L., Lo, C.H., Xu, X., Li, W.X., 2012. Magmatic switch-on and switch-off along the South China continental margin since the Permian: transition from an Andean-type to a western Pacific-type plate boundary. Tectonophysics 532–535 (3), 271-290.

Lister, G., & Baldwin, S. (1993). Plutonism and the origin of metamorphic core complexes. Geology, 21, 607-610.

Lister, G.S., Etheridge, M.A., Symonds, P.A., 1986. Detachment faulting and the evolution of passive continental margins. Geology 14, 246-250.

Liu, Q. H., Zhu, H. T., Shu, Y., Zhu, X. M., Yang, X. H., Chen, L., et al. (2016). Provenance identification and sedimentary analysis of the beach and bar systems in the Palaeogene of the Enping Sag, Pearl River Mouth Basin, South China Sea. Marine and Petroleum Geology, 70, 251-272. https://doi.org/10.1016/j.marpetgeo.2015.12.002

Lu, B.L., Wang, P.J., Zhang, G.C., Zhang, B., Sun, X.M., Li, W.Z., Lang, Y.Q., 2011. Basement structures of an epicontinental basin in the northern South China Sea and their significance in petroleum prospect. Acta Pet. Sin. 32 (4), 580-587 (in Chinese with English abstract).

Maestrelli, D., Montanari, D., Corti, G., Del Ventisette, C., Moratti, G., & Bonini, M. (2020). Exploring the interactions between rift propagation and inherited crustal fabrics through experimental modeling. Tectonics, 39(12), e2020TC006211. https://doi.org/10.1029/2020TC006211

McClay, K., White, M., 1995. Analogue modelling of orthogonal and oblique rifting. Mar. Pet. Geol. 12, 137-151.

Melosh, H. J. 1990. Mechanical basis for low-angle normal faulting in the Basin and Range province. Nature 343:331-335.

Metcalfe, I., 2006. Paleozoic and Mesozoic tectonic evolution and palaeogeography of East Asian crustal fragments: the Korean Peninsula in context. Gondwana Res. 9, 24-46.

Miller, E. L., Gans, P. B., & Garing, J., (1983). The snake range decollement; an exhumed mid-tertiary ductile-brittle transition. Tectonics, 2(3), 239-263.

Molnar, N. E., Cruden, A. R., & Betts, P. G. (2019). Interactions between propagating rifts and linear weaknesses in the lower crust. Geosphere, 15(5), 1617-1640.

Morley, C., Gabdi, S., & Seusutthiya, K. (2007). Fault superimposition and linkage resulting from stress changes during rifting: Examples from 3D seismic data, Phitsanulok Basin, Thailand. Journal of Structural Geology, 29(4), 646-663.

Morley, C., Haranya, C., Phoosongsee, W., Pongwapee, S., Kornsawan, A., & Wonganan, N. (2004). Activation of rift oblique and rift parallel preexisting fabrics during extension and their effect on deformation style: Examples from the rifts of Thailand. Journal of Structural Geology, 26(10), 1803-1829.

Morley, C.K., 2002. A tectonic model for the Tertiary evolution of strike-slip faults and rift basins in SE Asia. Tectonophysics 347, 189-215.

Morley, C.K., 2012. Late Cretaceous–Early Palaeogene tectonic development of SE Asia. Earth-Sci. Rev. 115, 37-75.

Muirhead, J. D., & Kattenhorn, S. A. (2017). Activation of preexisting transverse structures in an evolving magmatic rift in East Africa. Journal of Structural Geology, 106, 1-18.

Nanni, U. , Pubellier, M. , Chan, L. S. , & Sewell, R. J. . (2017). Rifting and reactivation of a cretaceous structural belt at the northern margin of the south china sea. Journal of Asian Earth Sciences, 136(APR.1), 110-123.

Numelin, T., Marone, C., Kirby, E., 2007. Frictional properties of natural gouge from a low-angle normal fault, Panamint Vallet, California. Tectonics 26, TC2004. http://dx.doi.org/10.1029/2005TC001916.

Odinsen, T., Reemst, P., Beek, P. V. D., Faleide, J. I., & Gabrielsen, R. H. (2000). Permo-Triassic and Jurassic extension in the northern North Sea: Results from tectonostratigraphic forward modelling. Geological Society, London, Special Publications, 167, 83-103.

Parsons, T. , & Thompson, G. A. . (1993). Does magmatism influence low-angle normal faulting?. Geology, 21(3).

Peacock, D., Sanderson, D., 1991. Displacements, segment linkage and relay ramps in normal fault zones. J. Struct. Geol. 13, 721-733.

Phillips, T. B., Jackson, A. L., Bell, R. E., Duffy, O. B., & Fossen, H. (2016). Reactivation of intrabasement structures during rifting: A case study from offshore southern Norway. Journal of Structural Geology, 91, 54-73.

Pigott, J. D., & Ru, K. (1994). Basin superposition on the northern margin of the South China Sea. Tectonophysics, 235(1-2), 27-50.

Proffett, J. M., Jr. 1977. Cenozoic geology of the Yerington District, Nevada, and implications for nature and origin of Basin and Range faulting. Geol. Soc. Am. Bull. 88:247-266.

Ranalli, G., & Yin, Z. M. (1990). Critical stress difference and orientation of faults in rocks with strength anisotropies: The two-dimensional case. Journal of Structural Geology, 12(8), 1067-1071.

Rangin, C., Huchon, P., Le Pichon, X., Bellon, H., Lepvrier, C., Roques, D., Hoe, N.D., Quynh, P.V., 1995. Cenozoic deformation of central and south Vietnam. Tectonophysics 1995, 179-196.

Ren, J.Y., Tamaki, K., Li, S.T., Junxia, Z., 2002. Late Mesozoic and Cenozoic rifting and its dynamic setting in Eastern China and adjacent areas. Tectonophysics 344, 175-205.

Rice, J., 1992. Fault stress states, pore pressure distributions, and the weakness of the San Andreas Fault. In: Evans, B., Wong, T.-F. (Eds.), Fault Mechanics and Transport Properties of Rocks; a Festschrift in Honor of W.F. Brace. Academic Press, San Diego, CA, pp. 475-503

Ring, U., 1994. The influence of preexisting structure on the evolution of the Cenozoic Malawi rift (east African rift system). Tectonics 13, 313-326.

Ru, K., & Pigott, J. D. (1986). Episodic rifting and subsidence in the South China Sea. AAPG Bulletin, 70(9), 1136-1155.

Samsu, A., Cruden, A. R., Molnar, N. E., & Weinberg, R. F. (2021). Inheritance of Penetrative Basement Anisotropies by Extension-Oblique Faults: Insights From Analogue Experiments. Tectonics, 40(5), e2020TC006596. https://doi.org/10.1029/2020TC006596

Scheiber, T., Viola, G., Bingen, B., Peters, M., Solli, A., 2015. Multiple reactivation and strain localization along a Proterozoic orogen-scale deformation zone: the Kongsberg-Telemark boundary in southern Norway revisited. Precambrian Res. 265, 78-103.

Schöpfer, M.P., Childs, C.,Walsh, J.J., 2006. Localisation of normal faults in multilayer sequences. Journal of Structural Geology 28, 816-833.

Sewell, R.J., Campbell, S.D.G., Fletcher, C.J.N., Lai, K.W., Kirk, P.A., 2000. The Pre-Quaternary Geology of Hong Kong. Geotechnical Engineering Office, Civil Engineering Department, the Government of the Hong Kong Special Administrative Region, p. 181.

Sewell, R.J., Tang, D.L.K., Campbell, S.D.G., 2012. Volcanic-plutonic connections in a tilted nested caldera complex in Hong Kong. Geochem. Geophys. Geosyst. 13, Q01006.

Shi, H.S., Dai, Y.D., Liu, L.H., Jiang, H., Li, H.B., Bai, J., 2015. Geological characteristics and distribution model of oil and gas reservoirs in Zhu I Depression, Pearl River Mouth Basin. Acta Pet. Sin. 36 (S2), 120-133.

Shi, H.S., Li, C.F., 2012. Mesozoic and early Cenozoic tectonic convergence-to-rifting transition prior to opening of the South China Sea. Int. Geol. Rev. 54 (15), 1801-1828.

Shu, L., Zhou, X., Deng, P., Wang, B., Jiang, S.-Y., Yu, J., Zhao, X., 2009. Mesozoic tectonic evolution of the southeast china block: new insights from basin analysis. J. Asian Earth Sci. 34, 376-391.

Shu, L.S., Faure, M., Jiang, S., Yang, Q., Wang, Y., 2006. SHRIMP zircon U–Pb age, litho- and biostratigraphic analyses of the Huaiyu Domain in South China. Episodes 29, 244-252.

Sibson, R. H. (1985). A note on fault reactivation. Journal of Structural Geology, 7(6), 751-754.

Soliva, R., Benedicto, A., Maerten, L., 2006. Spacing and linkage of confined normal faults: importance of mechanical thickness. J. Geophys. Res. 111 (B1), 17.

Sun, Z., Xu, Z., Sun, L., Pang, X., Yan, C., Li, Y., et al. (2014). The mechanism of post-rift fault activities in Baiyun sag, Pearl River Mouth basin. Journal of Asian Earth Sciences, 89, 76-87. https://doi.org/10.1016/j.jseaes.2014.02.018

Sun, Z., Zhou, D., Sun, L.T., Chen, C.M., Pang, X., Jiang, J.Q., Fan, H., 2010. Dynamic analysis on rifting stage of Pearl River Mouth Basin through Analogue Modeling. J. Earth Sci. 21, 439-454.

Sun, Z., Zhou, D., Wu, S.M., Zhong, Z.H., Myra, K., Jiang, J.Q., Fan, H., 2009. Patterns and dynamics of rifting on passive continental margin from shelf to slope of the northern South China Sea: evidence from 3D analogue modeling. J. Earth Sci. 20, 136-146.

Tapponnier, P., Lacassin, R., Leloup, P.H., Scharer, U., Zhong, D.L., Wu, H.W., Liu, X.H., Ji, S.C., Zhang, L.S., Zhong, J.Y., 1990. The Ailao Shan Red River Metamorphic Belt-Tertiary Left-Lateral Shear between Indochina and South China. Nature 343, 431-437.

Tapponnier, P., Peltzer, G., Ledain, A.Y., Armijo, R., Cobbold, P., 1982. Propagating extrusion tectonics in Asia – new insights from simple experiments with plasticine. Geology 10, 611-616.

Tapponnier, P., Xu, Z.Q., Roger, F., Meyer, B., Arnaud, N., Wittlinger, G., Yang, J.S., 2001. Geology – oblique stepwise rise and growth of the Tibet plateau. Science 294, 1671-1677.

Taylor, B., Hayes, D.E., 1980. The tectonic evolution of the South China Basin. In: Hayes, D.E. (Ed.), The Tectonic and Geologic Evolution of Southeast Asian Seas and Islands. Geophysical Monograph, pp. 89-104.

Taylor, B., Hayes, D.E., 1983. Origin and history of the South China Sea Basin. Washington Dc American Geophysical Union. Geophys. Monogr. 27, 23-56.

Walsh, J. J., Bailey, W. R., Childs, C., Nicol, A., & Bonson, C. G. (2003). Formation of segmented normal faults: A 3-D perspective. Journal of Structural Geology, 25(8), 1251-1262.

Walsh, J., Nicol, A., & Childs, C. (2002). An alternative model for the growth of faults. Journal of Structural Geology, 24(11), 1669-1675.

Wang, J. , Pang, X. , Liu, B. , Zheng, J. , & Wang, H. . (2018). The baiyun and liwan sags: two supradetachment basins on the passive continental margin of the northern south china sea. Marine and Petroleum Geology, 206-218.

Wang, L., Maestrelli, D., Corti, G., Zou, Y., & Shen, C. (2021). Normal fault reactivation during multiphase extension: Analogue models and application to the Turkana depression, East Africa. Tectonophysics, 811, 228870. https://doi.org/10.1016/j.tecto.2021.228870

Wang, Y.L., Qiu, Y., Yan, P., Zheng, H.B., Liu, H.L., Wang, J., 2016. Seismic evidence for Mesozoic strata in the northern Nansha waters, South China Sea. Tectonophysics 677, 190-198.

Wernicke, B., 1995. Low-angle normal faults and seismicity: a review. J. Geophys. Res. B, Solid Earth Planets100, 20159-20174.

Wernicke, B., and B.C. Burchfiel, 1982. Modes of extensional tectonics, J. Struct. Geol., 4, 105-115.

Wernicke, B., Axen, G., 1988. On the role of isostasy in the evolution of low-angle normal fault systems. Geology16, 848-851.

Wernicke, B., J. D. Walker, and M. S. Beaufait (1985), Structural discordance between Neogene detachments and frontal Sevier thrusts, central Mormon Mountains, southern Nevada, Tectonics, 4, 213-246.

Whipp, P., Jackson, C., Gawthorpe, R., Dreyer, T., & Quinn, D. (2014). Normal fault array evolution above a reactivated rift fabric; A subsurface example from the northern Horda Platform, Norwegian North Sea. Basin Research, 26(4), 523-549.

Willemse, E.J.M., Pollard, D.D., Aydin, A., 1996. Three-dimensional analyses of slip distributions on normal fault arrays with consequences for fault scaling. J. Struct. Geol. 18, 295-309.

Wong, M. S., and Gans, P. B. (2008), Geologic, structural, and thermochronologic constraints on the tectonic evolution of the Sierra Mazatán core complex, Sonora, Mexico: New insights into metamorphic core complex formation, Tectonics, 27, TC4013, doi:10.1029/2007TC002173.

Wu, S., Gao, J., Zhao, S., Lüdmann, T., Chen, D., & Spence, G. (2014). Post-rift uplift and focused fluid flow in the passive margin of northern South China Sea. Tectonophysics, 615, 27-39. https://doi.org/10.1016/j.tecto.2013.12.013

Xiao, H. B., F. A. Dahlen, and J. Suppe. 1991. Mechanics of extensional wedges, J. Geophys. Res., 96: 10, 301-310, 318.

Xu, X.M., Chen, S.H., Wang, F.G., Hu, K., Yu, S.M., Wang, X.C., Gao, Z.L., Liu, X.L., 2014. Structural features and its impacts on hydrocarbon accumulation of Neogene in Enping Sag, Pearl River Mouth Basin. Geoscience 28 (03), 543-550 (in Chinese with English abstract).

Yan, P., Liu, H.L., 2004. Tectonic-stratigraphic division and blind fold structures in Nansha Waters, South China Sea. J. Asian Earth Sci. 24 (3), 337-348.

Yan, P., Wang, L.L., Wang, Y.L., 2014. Late Mesozoic compressional folds in Dongsha Waters, the northern margin of the South China Sea. Tectonophysics 615, 213-223.

Ye, Q. , Mei, L. , H Shi, Du, J. , Deng, P. , & Shu, Y. , et al. (2020). The influence of pre-existing basement faults on the cenozoic structure and evolution of the proximal domain, northern south china sea rifted margin. Tectonics, 39(3).

Ye, Q., Mei, L., Shi, H., Shu, Y., Camanni, G., & Wu, J. (2018). A low-angle normal fault and basement structures within the Enping Sag, Pearl River Mouth Basin: Insights into late Mesozoic to early Cenozoic tectonic evolution of the South China Sea area. Tectonophysics, 731, 1-16. https://doi.org/10.1016/j.tecto.2018.03.003

Yi, H., Zhang, L., Lin, Z., 2012. Mesozoic tectonic framework and basin distribution characteristics of northern margin of South China Sea. Pet. Geol. Exp. 34 (4), 388-394 (in Chinese with English abstract).

Yin, A. 1989. Origin of regional rooted low-angle normal faults: a mechanical model and its implications. Tectonics 8:469-482.

Yin, A., Dunn, J., 1992. Structural and stratigraphic development of the Whipple–Chemehuevi detachment system, southeastern California: implications for the geometrical evolution of domal and basinal low-angle normal faults. Geol. Soc. Am. Bull.104, 659-674.

Zhou, D., Ru, K., Chen, H.Z., 1995. Kinematics of Cenozoic extension on the South China Sea continental margin and its implications for the tectonic evolution of the region. Tectonophysics 251, 161-177.

Zhou, D., Wang, W.Y., Wang, J.L., Pang, X., Cai, D.S., Sun, Z., 2006. Mesozoic subduction–accretion zone in northeastern South China inferred from geophysical interpretations. Sci. Chin. Ser. D 49, 471-482.

Zhou, X., Li, W., 2000. Origin of late Mesozoic igneous rocks in southeastern china: implications for lithosphere subduction and underplating of mafic magmas. Tectonophysics 326, 269-287.

Zhou, Z., Mei, L., Shi, H. et al. Evolution of Low-Angle Normal Faults in the Enping Sag, the Northern South China Sea: Lateral Growth and Vertical Rotation. J. Earth Sci. 30, 1326-1340 (2019). https://doi.org/10.1007/s12583-019-0899-4.

Zhu, W.L., Jiang, W.R., 1998. Relations between fractures and hydrocarbon reservoirs in Weixinan sag. Acta Petrol. Ei Sin. 19, 6-10 (in Chinese with English abstract).

Zwaan, F., & Schreurs, G. (2017). How oblique extension and structural inheritance influence rift segment interaction: Insights from 4D analog models. Interpretation, 5(1), SD119-SD138. https://doi.org/10.1190/INT-2016-0063.1

Zwaan, F., Chenin, P., Erratt, D., Manatschal, G., & Schreurs, G. (2021). Complex rift patterns, a result of interacting crustal and mantle weaknesses, or multiphase rifting? Insights from analogue models. Solid Earth, 12, 1473–1495, 2021

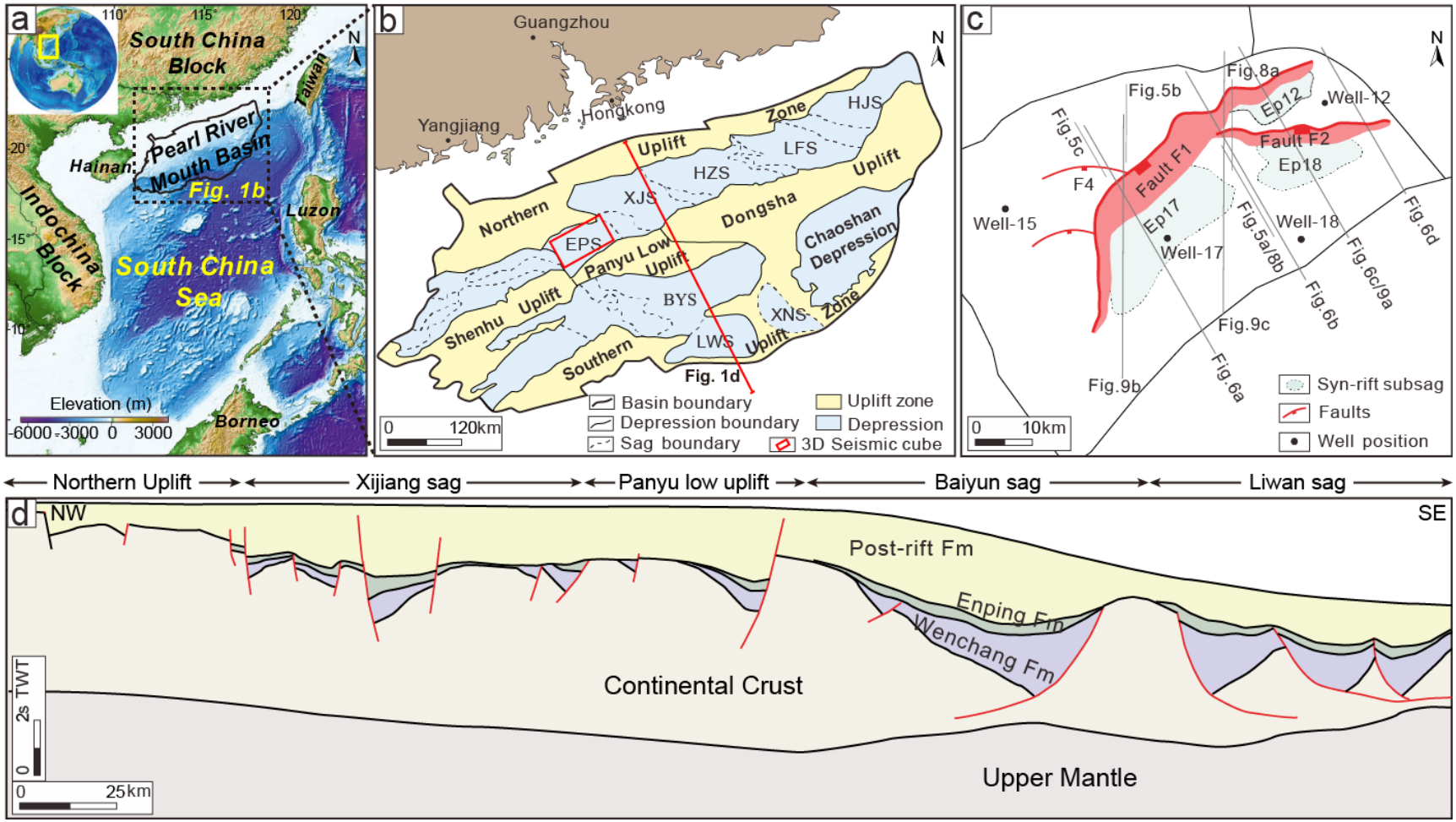

Fig. 1 Location and simplified structural map of the study area. (a) Topography and bathymetry of the South China Sea and adjacent regions. (b) Map of structural divisions of the Pearl River Mouth Basin and location of the Enping Sag. EPS—Enping Sag; XJS—Xijiang Sag; HZS—Huizhou Sag; LFS—Lufeng Sag; HJS—Hanjiang Sag; BYS—Baiyun Sag; LWS—Liwan Sag; XNS—Xingning Sag. (c) Schematic structural map and depocenter of the Enping sag at the basement. Straight lines show the location of cross-sections. (d) Transect across the middle part of the Pearl River Mouth Basin, showing the geological interpretation of the structure of the northern South China Sea margin. After Yang et al. (2018); Ye et al. (2018).

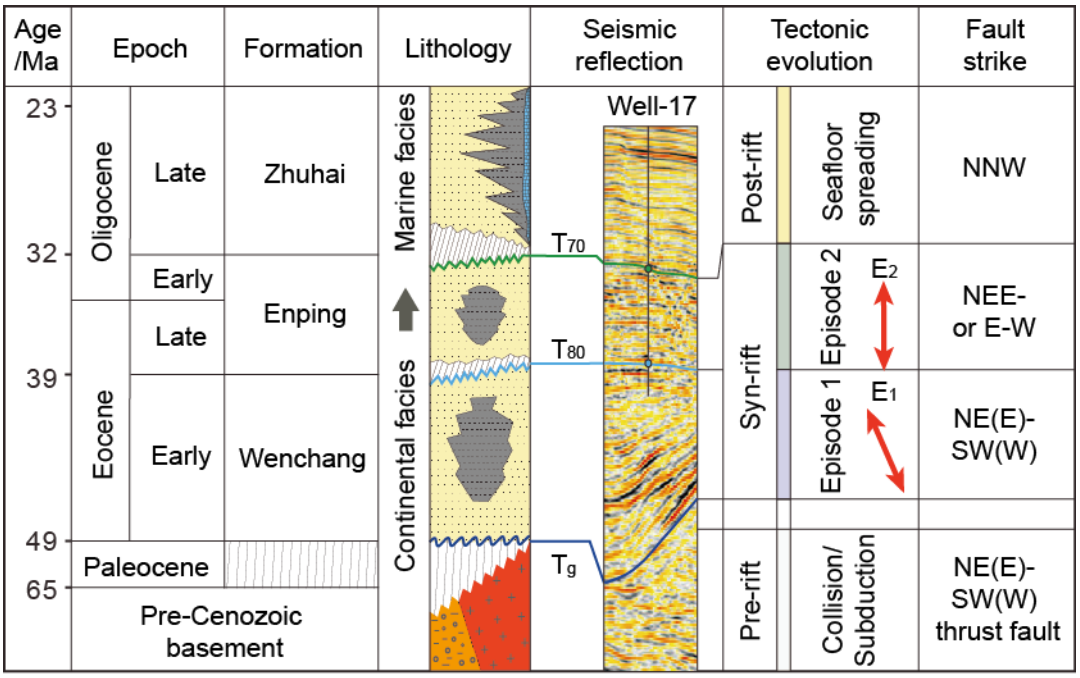

Fig. 2 Tectono-Stratigraphic evolution column of the Pearl River Mouth Basin, showing the geological correlation with seismic section and the key seismic horizons interpreted throughout this study, along with the major tectonic events to have affected the region. After Ye et al. (2018). Colours of horizons and stratigraphic intervals are consistent and referred to throughout the text. Red arrow represents the extension direction of each rift episode.

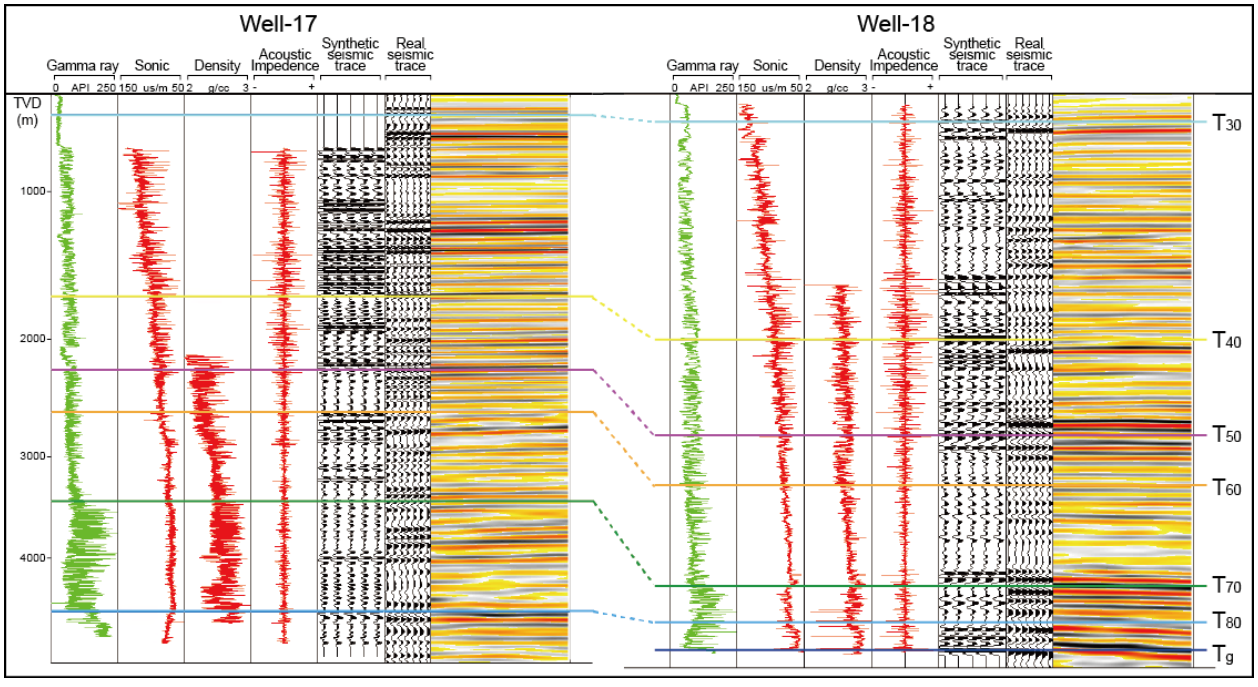

Fig. 3 Seismic-well ties for Well-17 and Well-18. See Fig. 1c for the location of the wells. Seismic data are Normal Polarity (SEG Convention), whereby a peak (brown reflection) represents an increase in acoustic impedance and a trough (black reflection) a decrease in acoustic impedance. T_{30} to T_{60} are correlated seismic horizons in the Pearl River Mouth Basin, and T_{70} to T_g are the key seismic horizons interpreted in the study area.

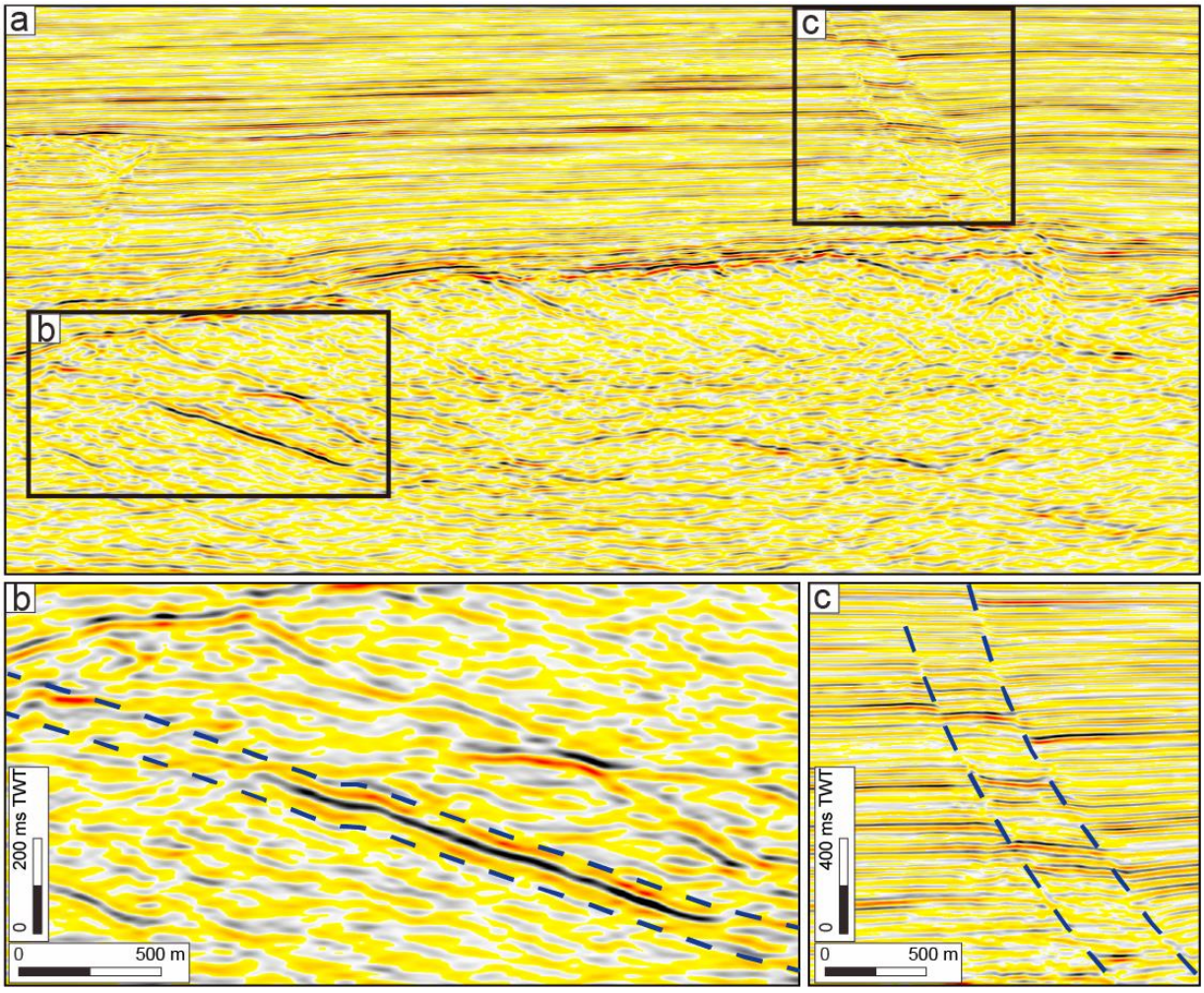

Fig. 4 Methods of interpreting intrabasement and rift-related structures. (a) Cross-section showing the observed fault structures in the stratigraphic cover and basement rocks. (b) A close-up showing the observed thin intrabasement reflection packets, and (c) A close-up showing the interpretating method of rift-related fault structure.

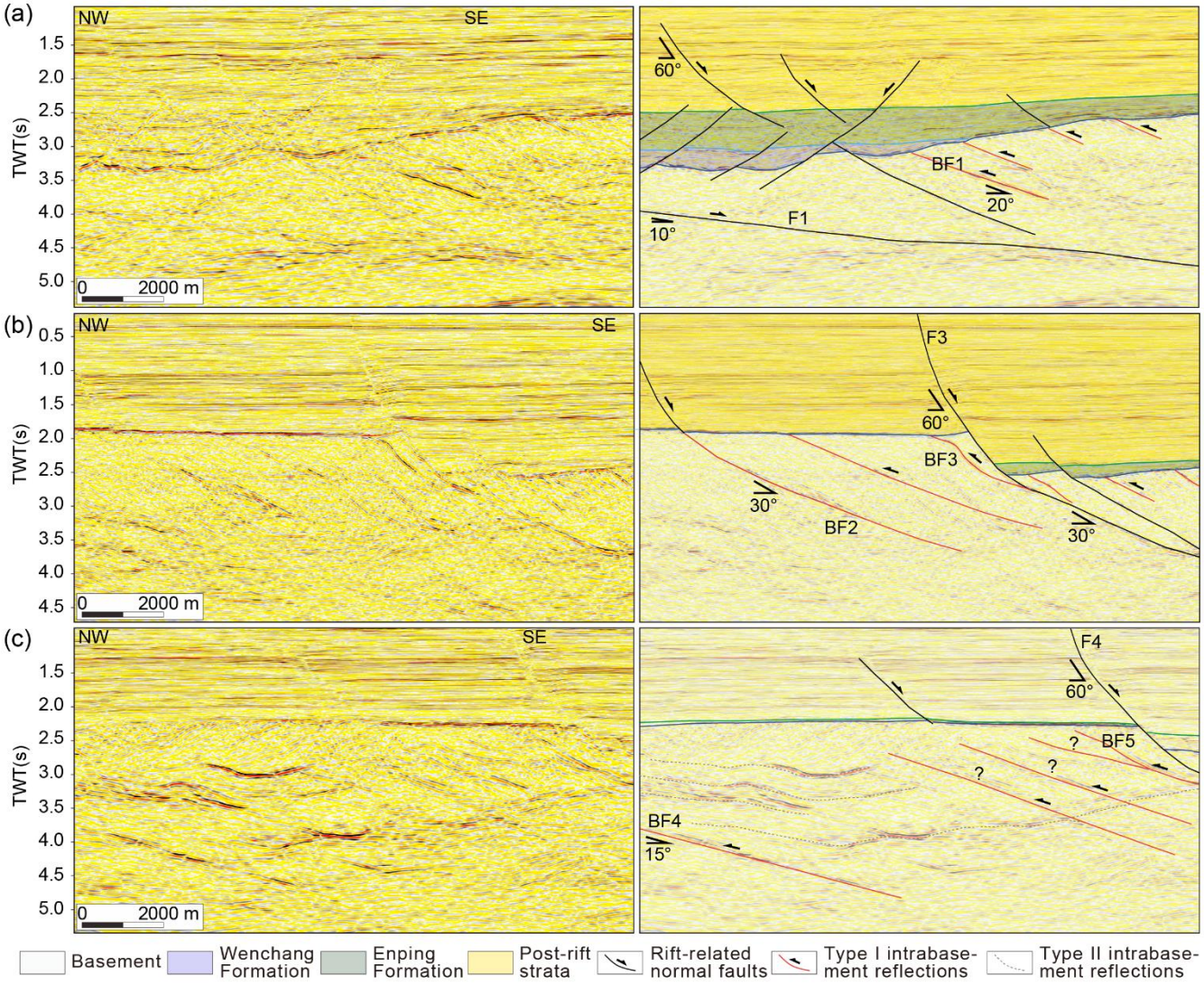

Fig. 5 Uninterpreted (Left panels) and interpreted (Right panels) cross-sections showing the occurrence of intrabasement structures in the study area. (a) and (b) show the characteristics of Type I intrabasement structure, while (c) shows the interpretation of Type II intrabasement structure with Type I intrabasement structure. Question mark indicates uncertainty of the interpretation. See Fig. 1 for location. Colours within the sedimentary cover correspond to ages shown within the stratigraphic column (Fig. 2)

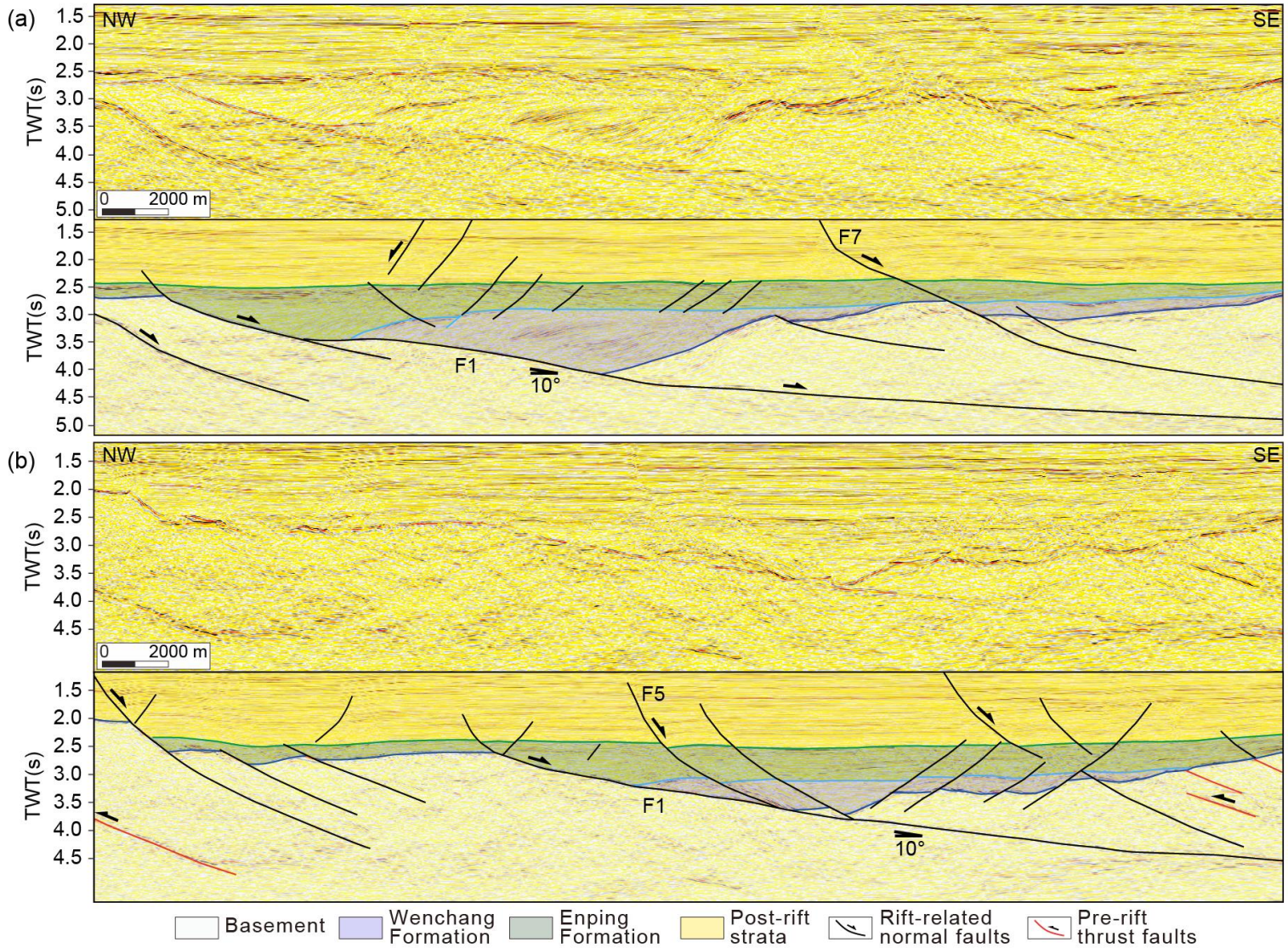

Fig. 6 Cross-sections perpendicular to the major structural trend showing the geometry of the major fault F1 and hanging-wall half-graben. (a)-(d) are four uninterpreted and interpreted cross-sections sub-perpendicular to the local strike across fault F1, with the simplified interpretation of stratigraphy. The colours used for the key horizons and stratigraphic intervals between them are consistent with those used in Fig. 2. See Figs. 1 for location.

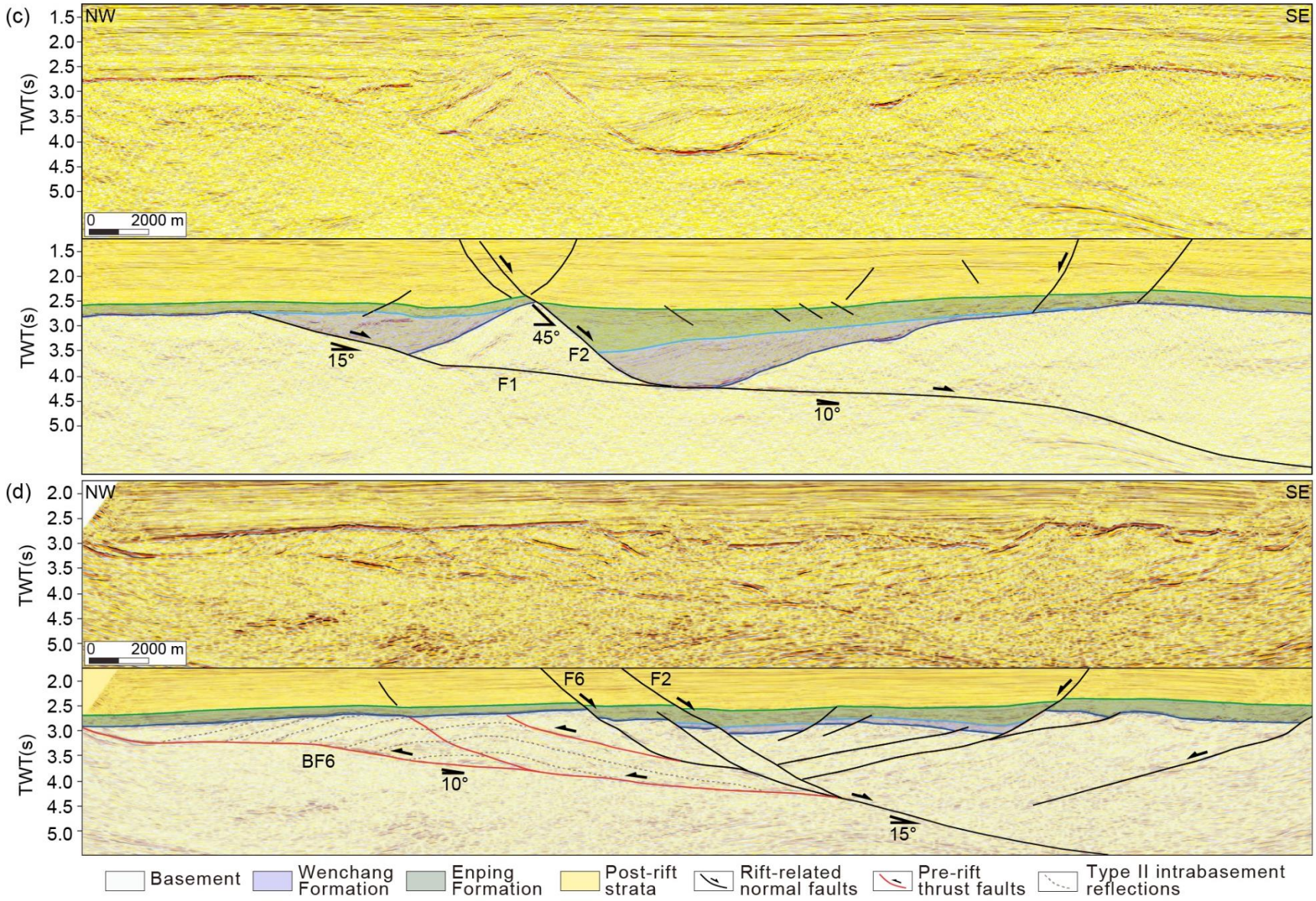
(c)
NW
SE
TWT(s)
1.5
2.0
2.5
3.0
3.5
4.0
4.5
5.0
0
2000 m
15°
45°
F2
F1
10°
(d)
NW
SE
TWT(s)
2.0
2.5
3.0
3.5
4.0
4.5
5.0
0
2000 m
F6
F2
BF6
10°
15°
Basement
Wenchang Formation
Enping Formation
Post-rift strata
Rift-related normal faults
Pre-rift thrust faults
Type II intrabasement reflections

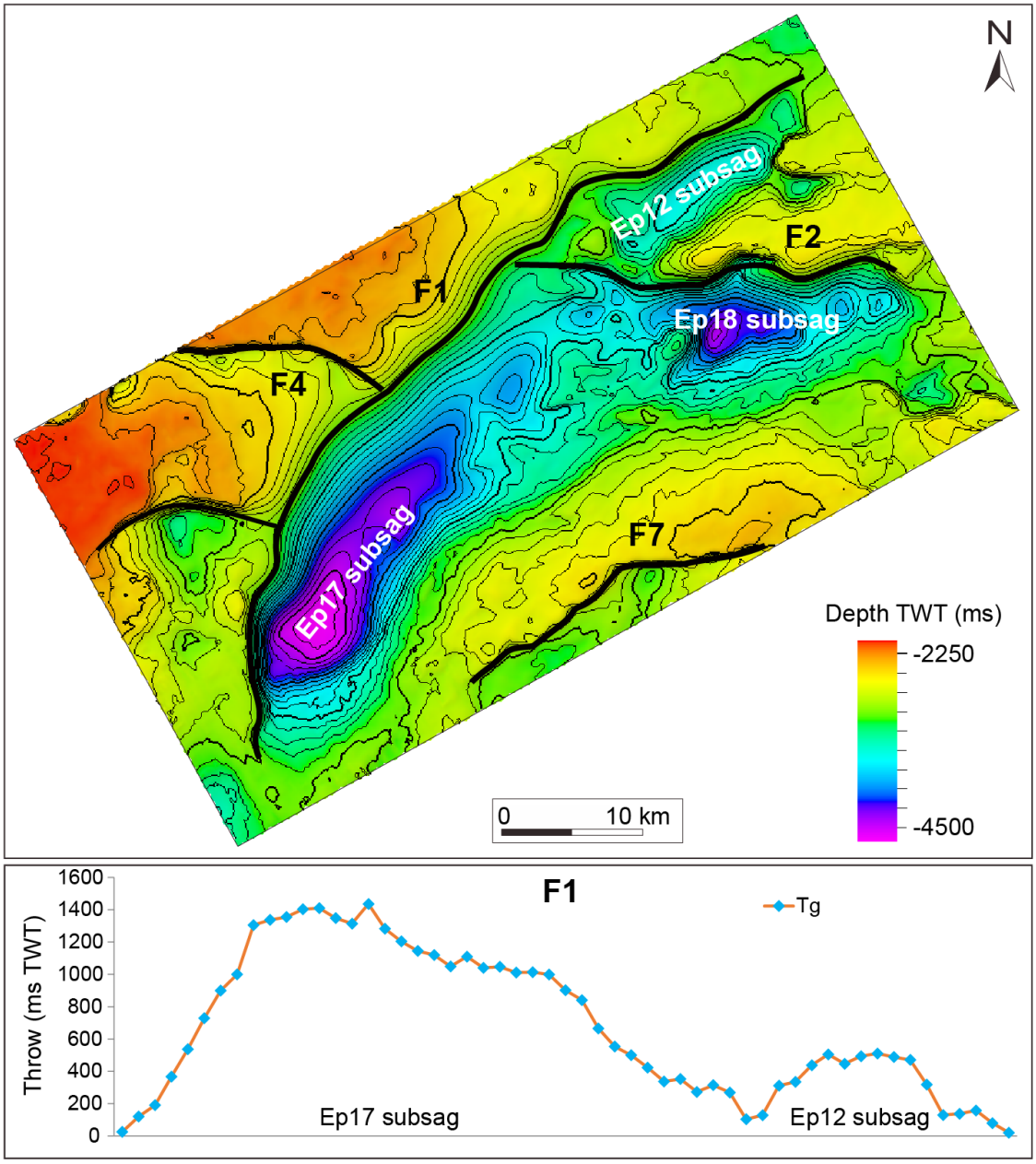

Fig. 7 Upper panel is the TWT structure map of the top basement showing the location of key fault traces and sub-sags. Color bar shows the depth of the top basement from the ground. Red is the uplift, purple is the depocenter. Lower panel shows the T-x plots of the major fault F1.

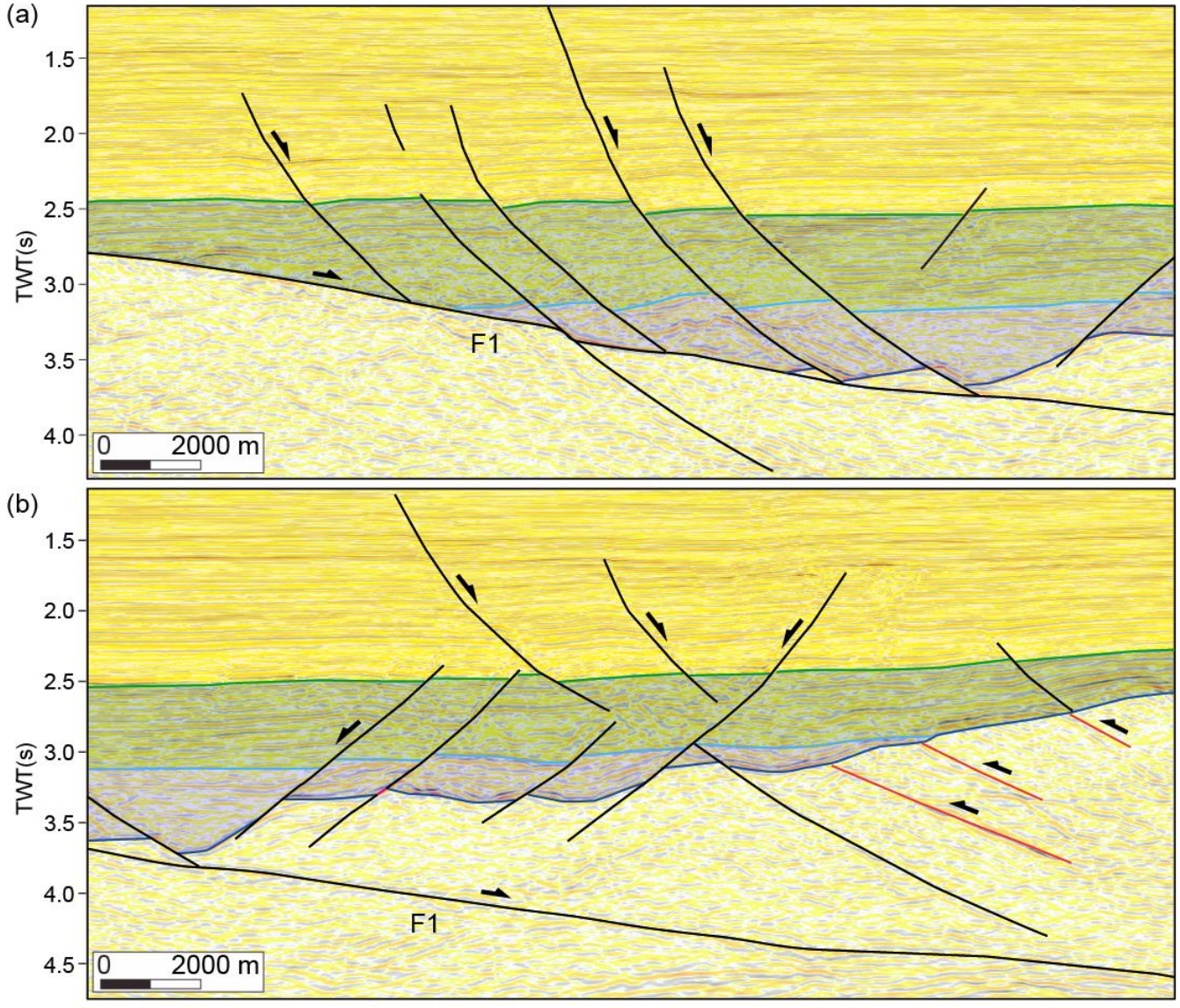

Fig. 8 Cross-sections showing the assemblage style of minor faults. (a) Domino faults developing on the slipping plane of the major fault F1. (b) Conjugate fault developing on the gentle slope of the Enping sag. See Figs. 1 for location.

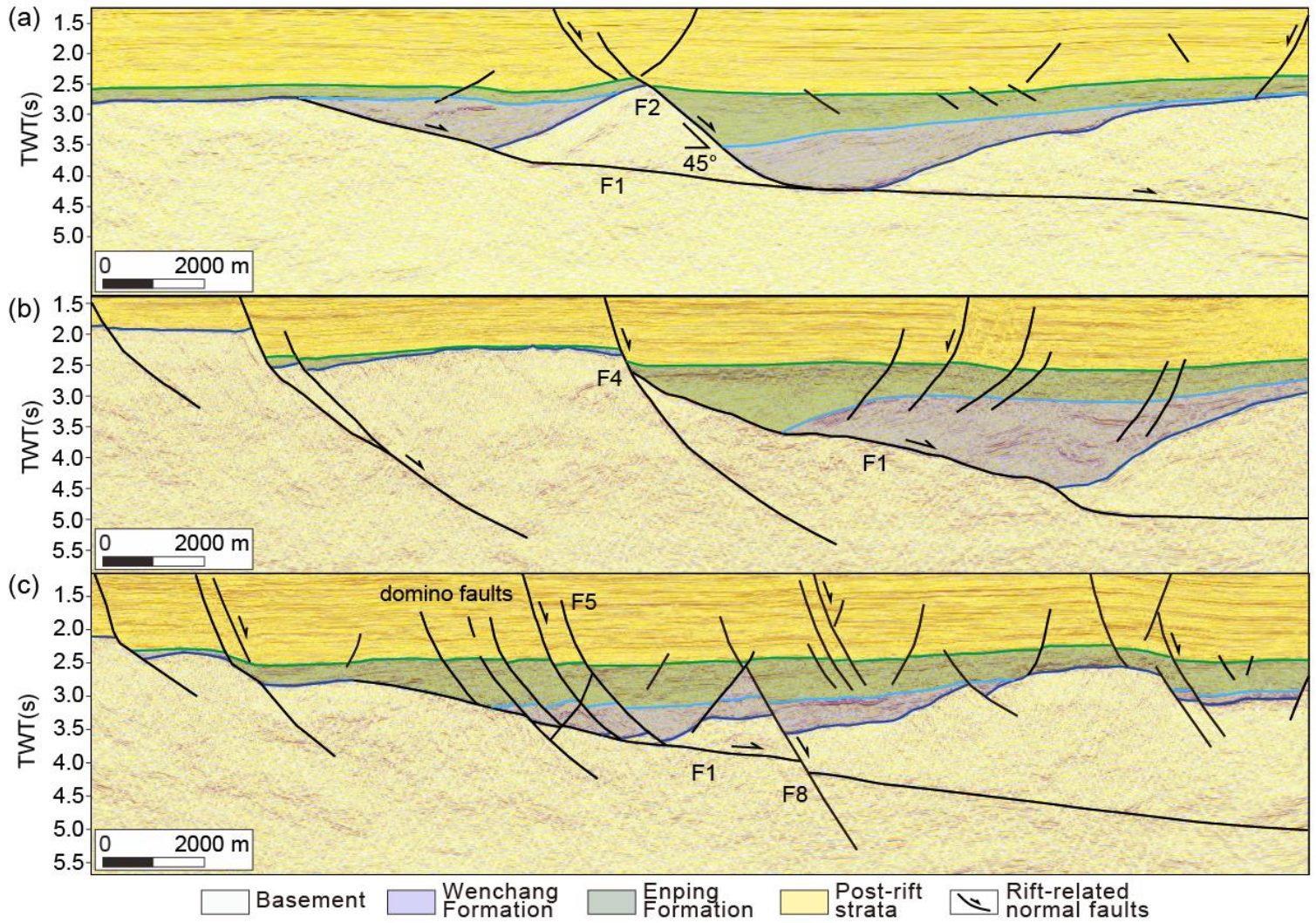

Fig. 9 Cross-sections showing interaction styles between the low-angle major fault and high-angle faults found in the Enping sag. (a) 'Merging faults' that join together at the lower tips (F1 and F2). (b) 'Abutting fault' that initiates at the low-angle normal fault (F1 and F4). (c) 'Abutting fault' (F1 and F5) and (d) 'Cross-cutting fault' that offsets the low-angle normal fault (F1 and F8). See Figs. 1 for location.

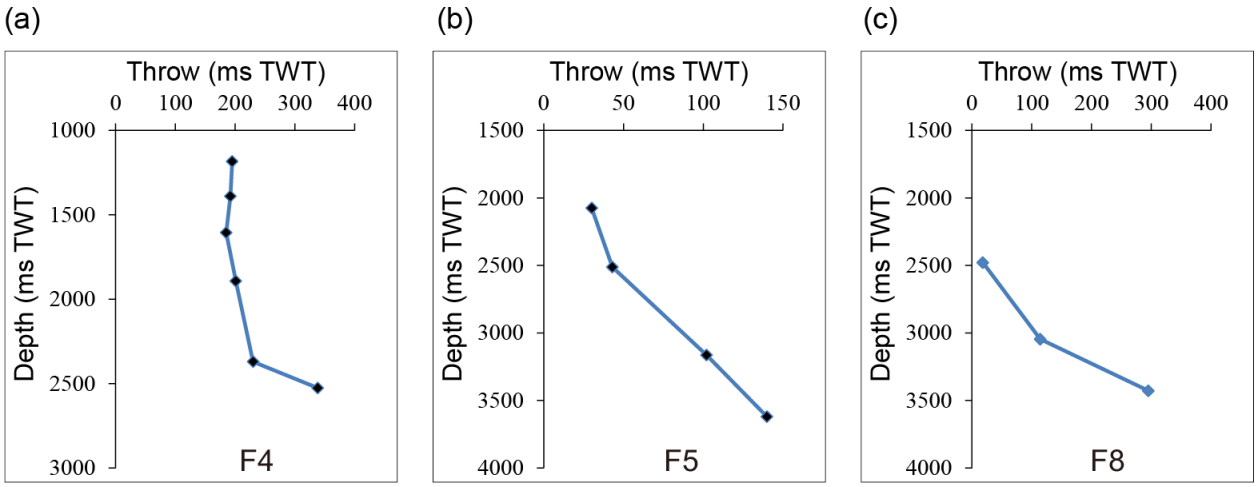

Fig. 10 T-z profiles of fault F4, F5 and F8.

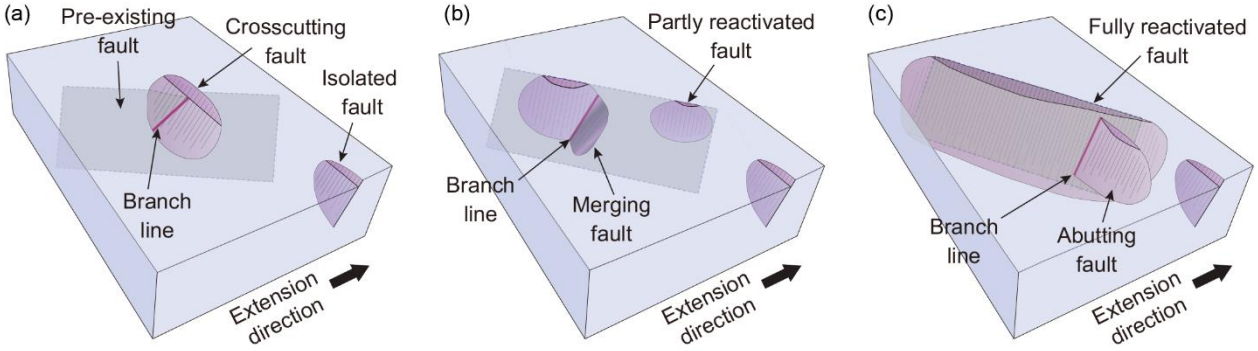

Fig. 11 Summary figure showing the variety in the reactivation mode of pre-existing thrust fault and fault interaction styles developing during later rifting. (a) No reactivation. (b) Partial reactivation. (d) Full reactivation. Grey rectangle is pre-existing thrust fault existing beneath the surface. Purple oval is new fault. Black fault traces indicate the surface expressions of faults. Purple line is the branch line at the intersection between fault pairs.

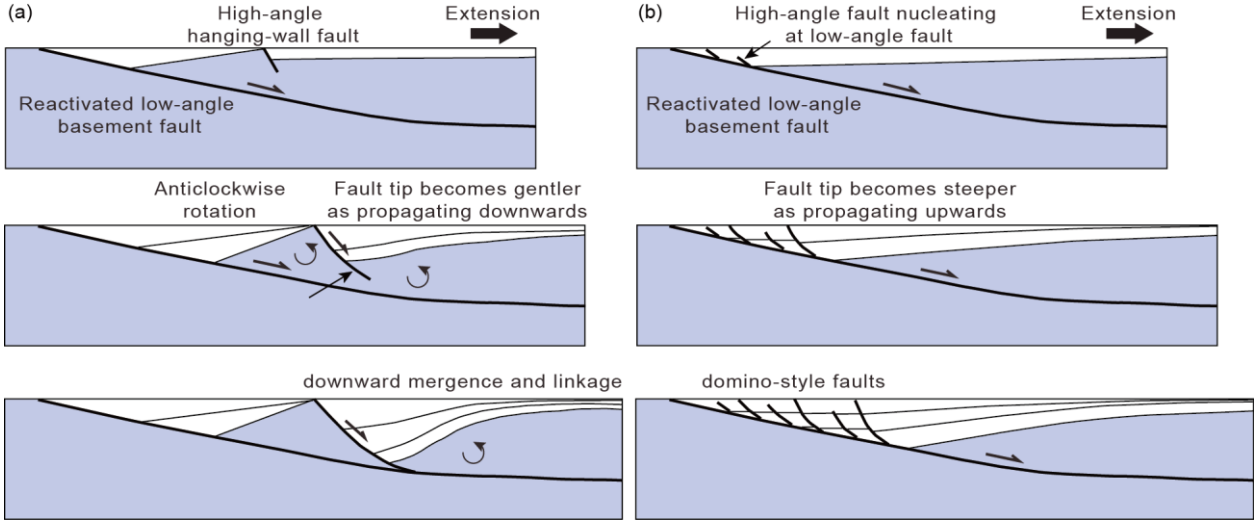

Fig. 12 Model of fault evolution between reactivated basement thrust and newly-formed high-angle normal faults during rifting. (a) 'Decoupled model' that that reactivated thrust fault and nearby new faults are initially isolated, followed by a later stage of vertical propagation and final linkage to form a connect fault system (b) 'Coupled model' that new faults nucleate at reactivated fault and grow as kinematically related components of a fault array, where the reactivated thrust fault serves as nucleation sites of new faults.

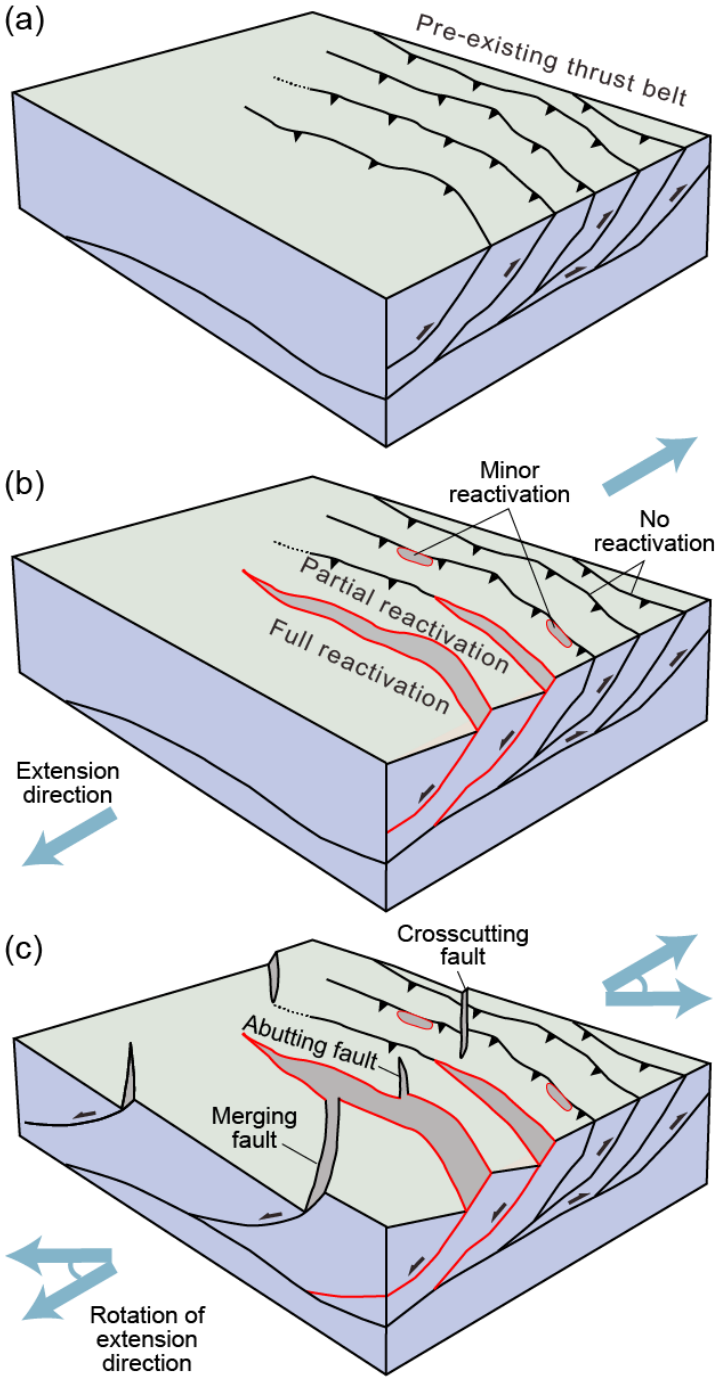

Fig. 13 Synoptic figure showing how the presence of basement thrusting structures may influence the geometry and evolution of overlying rift system. (a) Pre-rift framework of thrusting structures within crystalline basement. (b) Upon orthogonal extension those pre-rift thrusts act to control the reactivation extent, location and degree of faulting, and basin-boundary fault that occurs during rifting. (c) Subsequent rotation of extension direction produces a range of interactions with the rift-related faults, affecting the overall basin structures and paleotopography.